Supporting Information

Manifestation of Structural Differences of Atomically Precise Cluster Assembled Solids in Their Mechanical Properties

Korath Shivan Sugi,[a] Payel Bandyopadhyay,[b] Mohammad Bodiuzzaman,[a] Abhijit Nag,[a] Manjapoyil Hridya,[a] Wakeel Ahmed Dar,[a] Pijush Ghosh,*[b] and Thalappil Pradeep*[a]

[a] *DST Unit of Nanoscience (DST UNS) and Thematic Unit of Excellence (TUE), Department of Chemistry, Indian Institute of Technology Madras, Chennai 600 036, India*

[b] *Department of Applied Mechanics, Indian Institute of Technology Madras, Chennai 600036, India.*

**E-mail:* pijush@iitm.ac.in and pradeep@iitm.ac.in

Table of contents

Table S1. Structural parameters of the cluster single crystals tested.

Cluster	Ligand	Crystal system	Density	Z
$Ag_{29}(BDT)_{12}(TPP)_4$	1,3 Benzene dithiol	Cubic 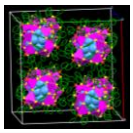	2.116 g/cm^{-3}	8
$Ag_{29}(BDT)_{12}(TPP)_4$	1,3 Benzene dithiol	Trigonal 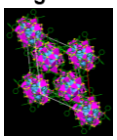	2.041 g/cm^{-3}	6
$Ag_{46}(DMBT)_{24}(TPP)_8$	2,5 Dimethyl benzene thiol	Trigonal 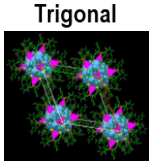	1.322 g/cm^{-3}	1
$Ag_{40}(DMBT)_{24}(TPP)_8$ + $Ag_{46}(DMBT)_{24}(TPP)_8$	2,4 Dimethyl benzene thiol	Monoclinic 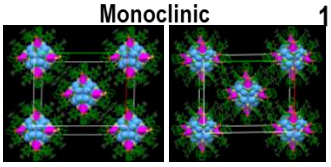	1.497 g/cm^{-3}	2

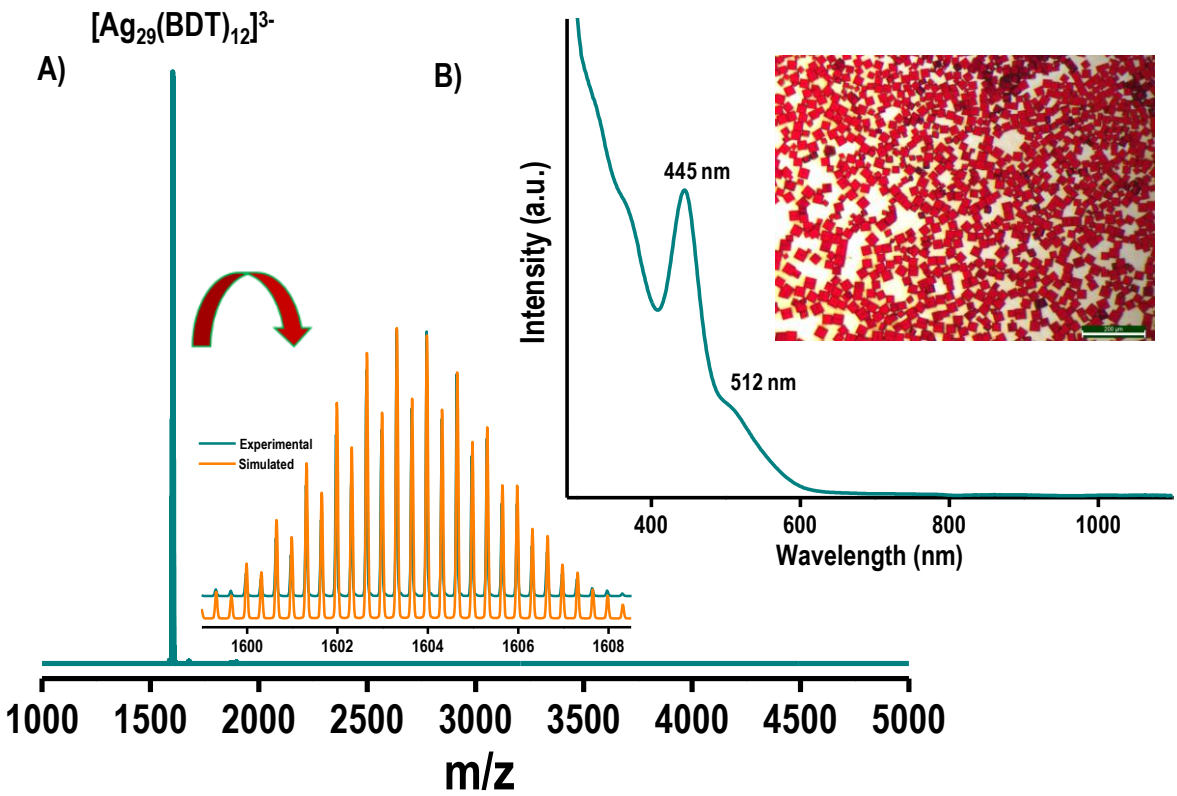

Figure S1. Characterization of Ag_{29} C clusters. A) Full range ESI MS of $Ag_{29}(BDT)_{12}(TPP)_4$ clusters in negative mode. Inset shows the comparison of experimental (cyan trace) and

simulated (orange trace) isotopic distributions of the cluster. B) UV-vis absorption spectrum of the $Ag_{29}(BDT)_{12}(TPP)_4$ cluster in dimethylformamide (DMF). Inset of the B shows the optical images of Ag_{29} C crystals collected in the transmission mode.

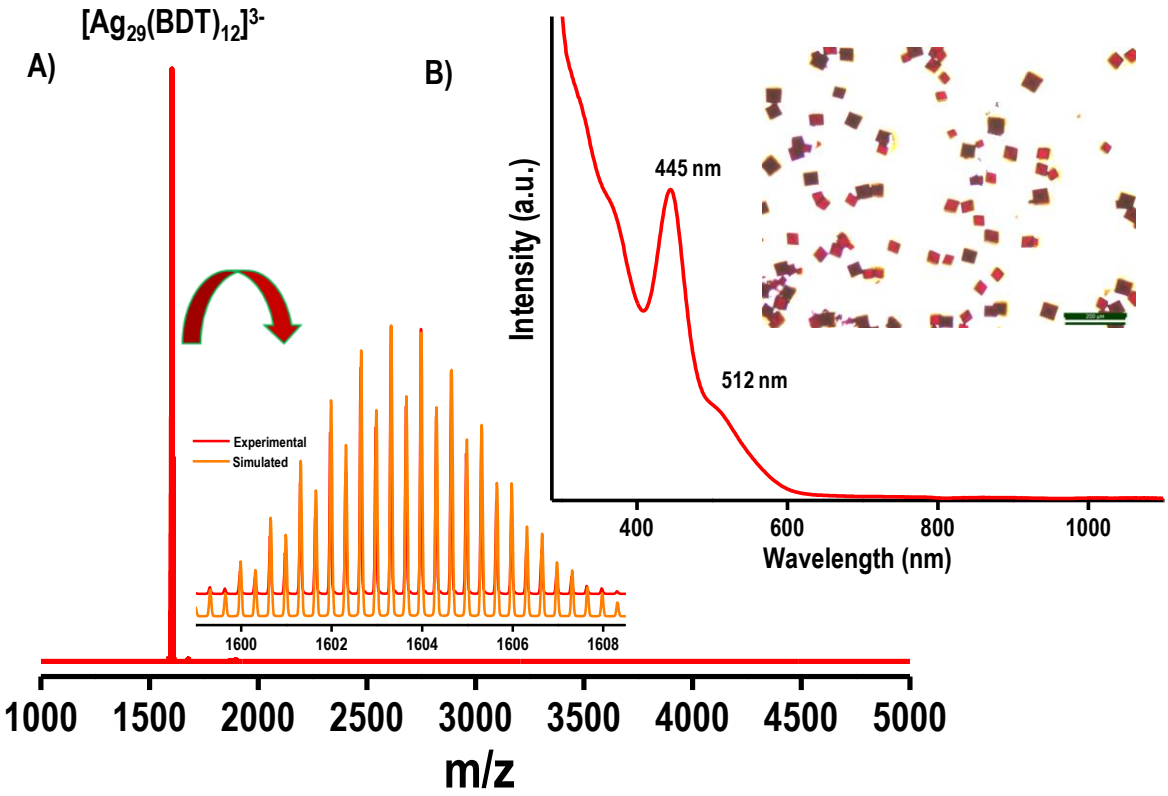

Figure S2. Characterization of Ag_{29} T clusters. A) Full range ESI MS of $Ag_{29}(BDT)_{12}(TPP)_4$ clusters in negative mode. Inset shows the comparison of experimental (red trace) and simulated (orange trace) isotopic distributions of the cluster. B) UV-vis absorption spectrum of the $Ag_{29}(BDT)_{12}(TPP)_4$ cluster in DMF. Inset of the B shows the optical images of Ag_{29} T crystals collected in transmission mode.

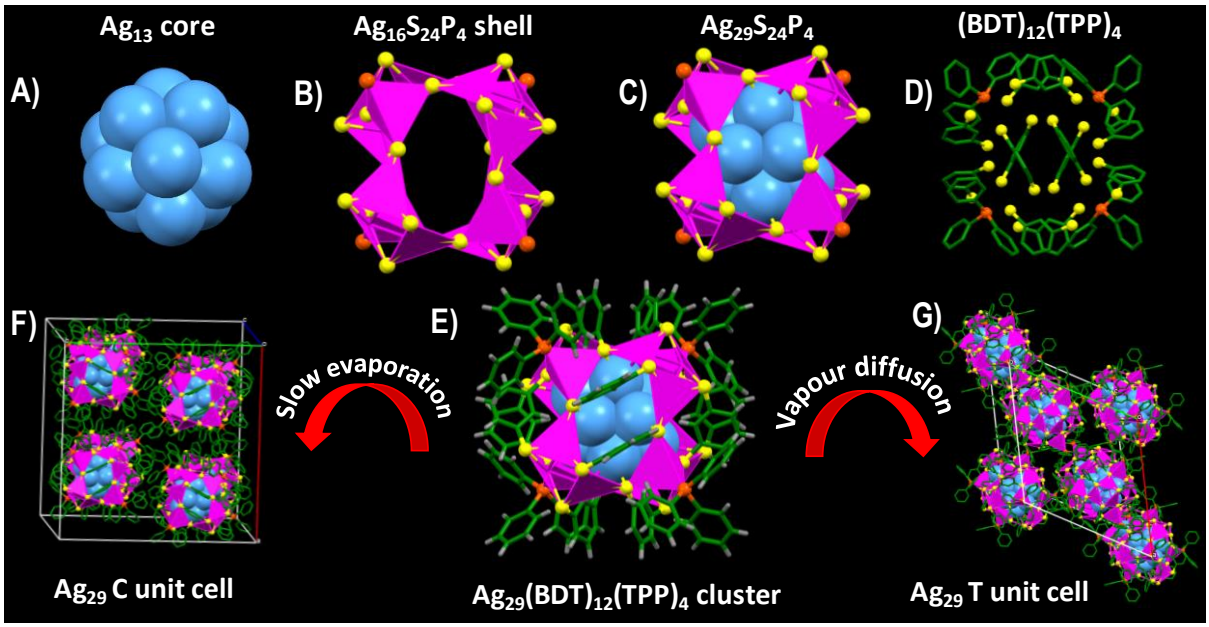

Figure S3. Structural anatomy of Ag_{29} C and T clusters. A) Ag_{13} centred icosahedral core; B) $Ag_{16}S_{24}P_4$ shell; C) $Ag_{29}S_{24}P_4$ motifs where the ligands are omitted for clarity. D) The packing of BDT and TPP ligands in an Ag_{29} cluster. E) Total structure of $Ag_{29}(BDT)_{12}(TPP)_4$ cluster. F) and G) are the unit cell packing of Ag_{29} C and Ag_{29} T. Color codes: cerulean/magenta, Ag; yellow, S; orange, P; green, C; grey, H.

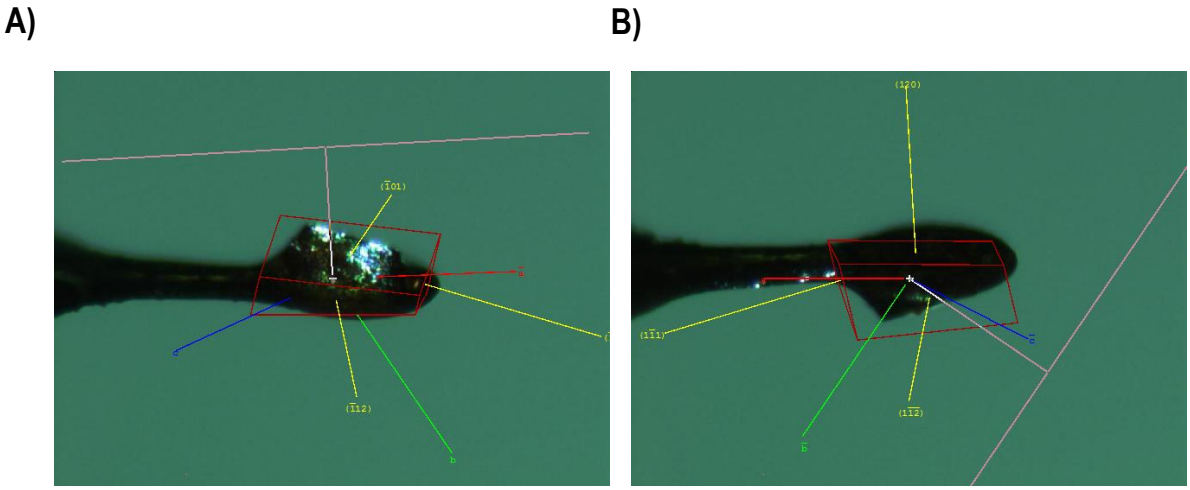

Figure S4. Face index analysis of Ag_{29} T based on single crystal X-ray crystallography. The crystal is mounted on MiTeGen loop.

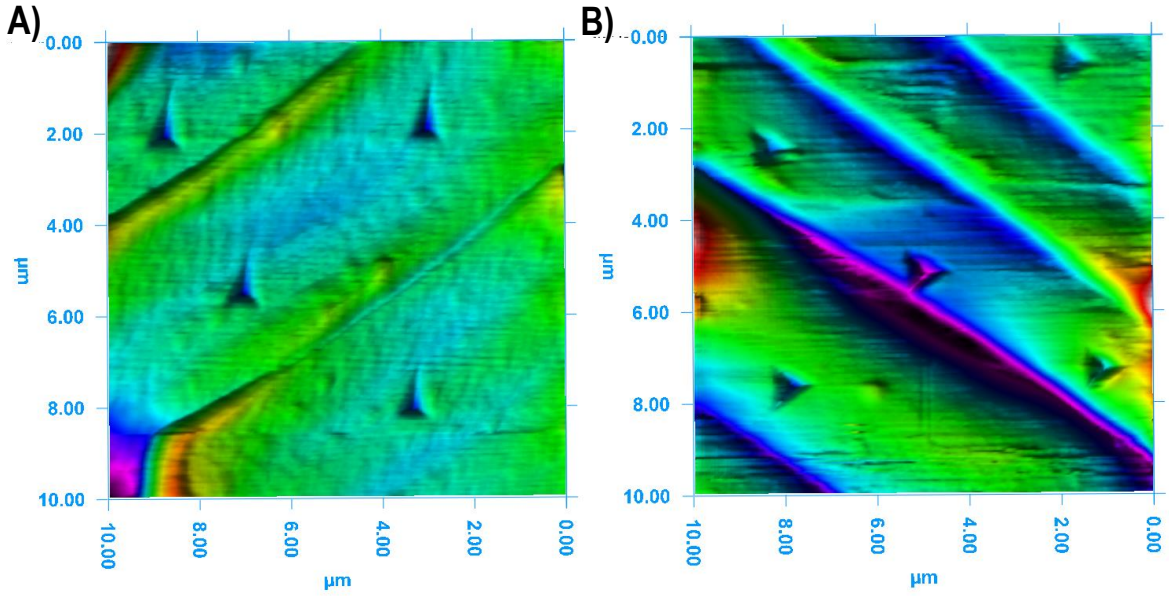

Figure S5. Piezo images showing residual indentation imprint on A) Ag_{29} C and B) Ag_{29} T crystals.

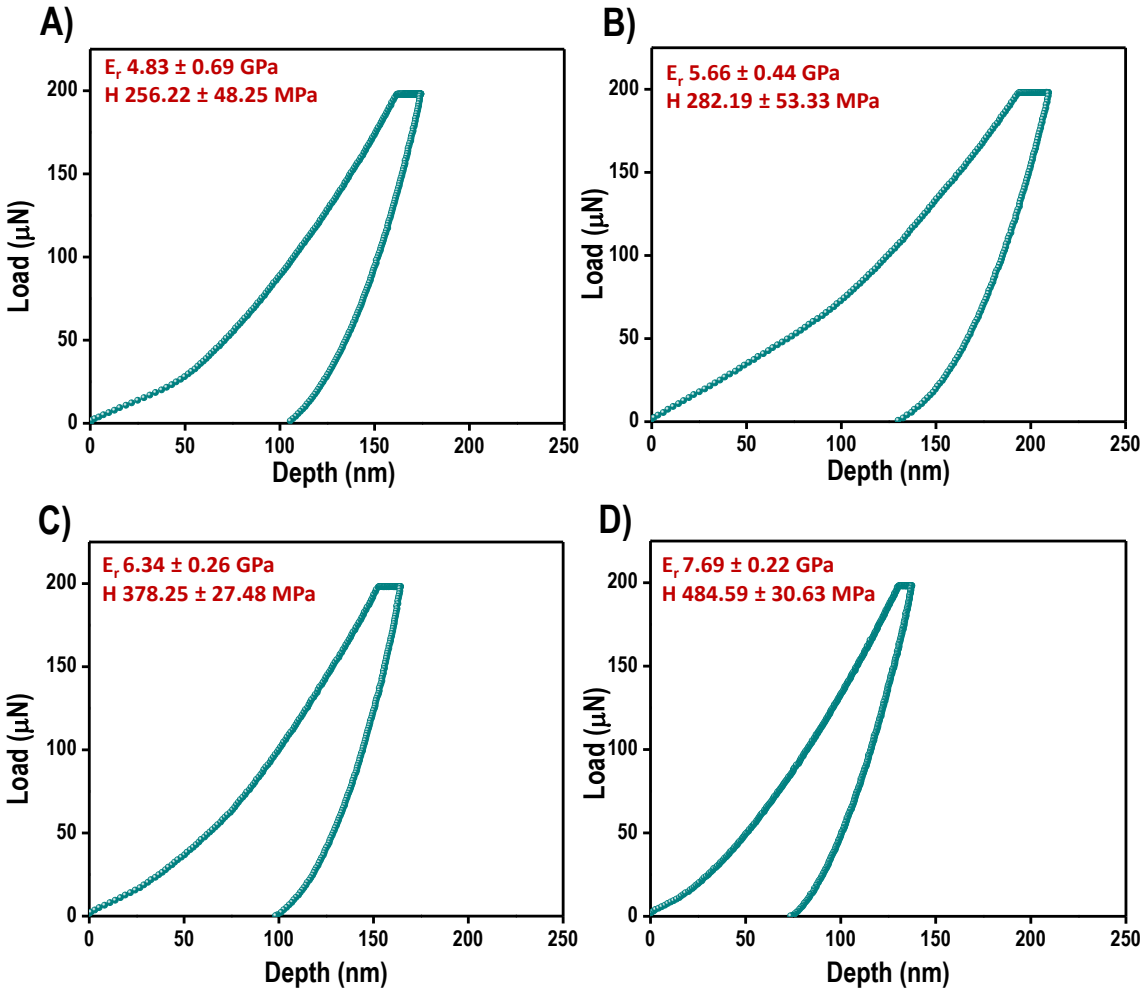

Figure S6. Load-displacement curves of Ag_{29} C crystals with loading rates of A) 20, B) 10, C) 6.6, and D) 4 µN/s, respectively.

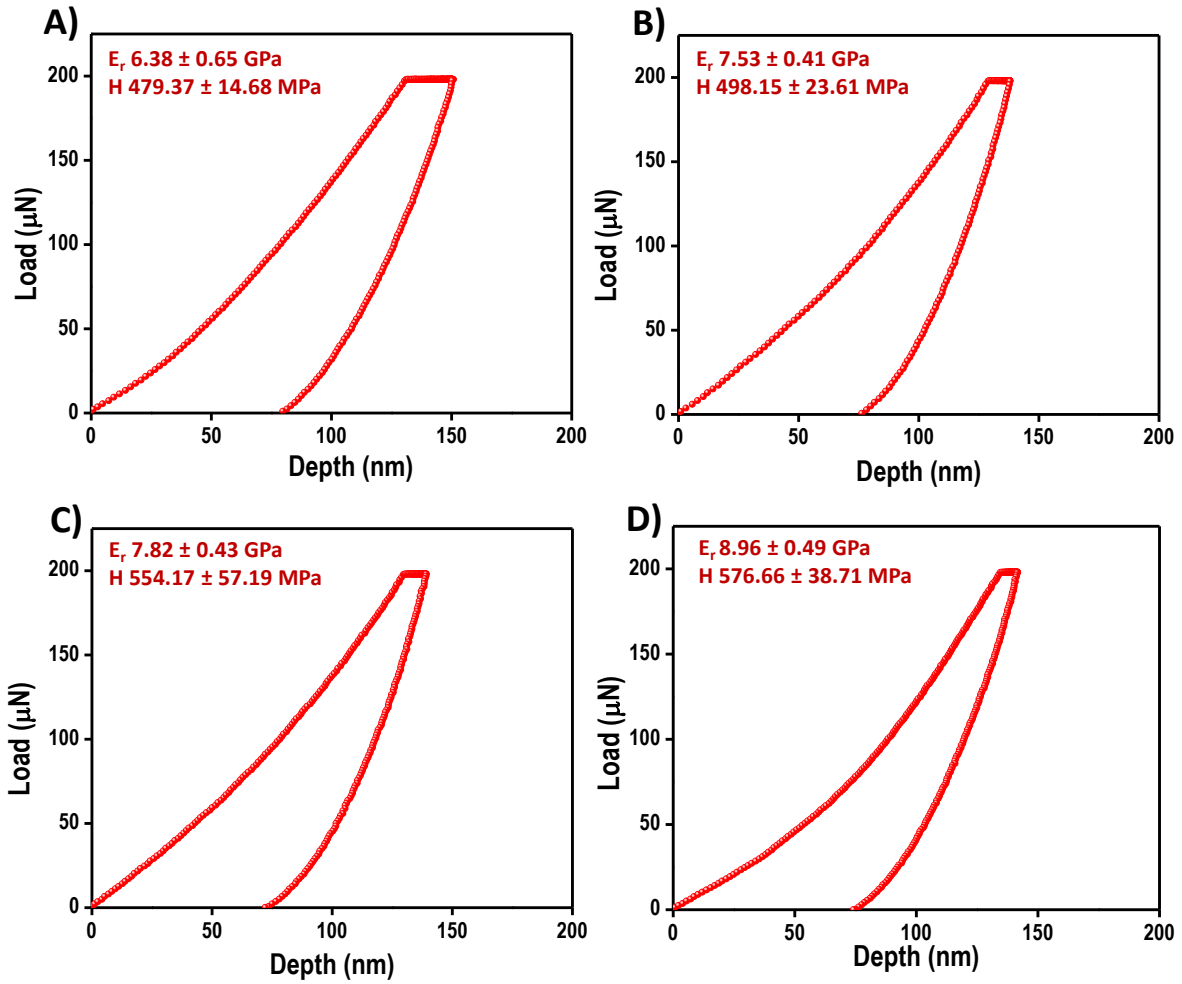

Figure S7. Load-displacement curves of Ag_{29} T crystals with loading rates of A) 20, B) 10, C) 6.6, and D) 4 µN/s, respectively.

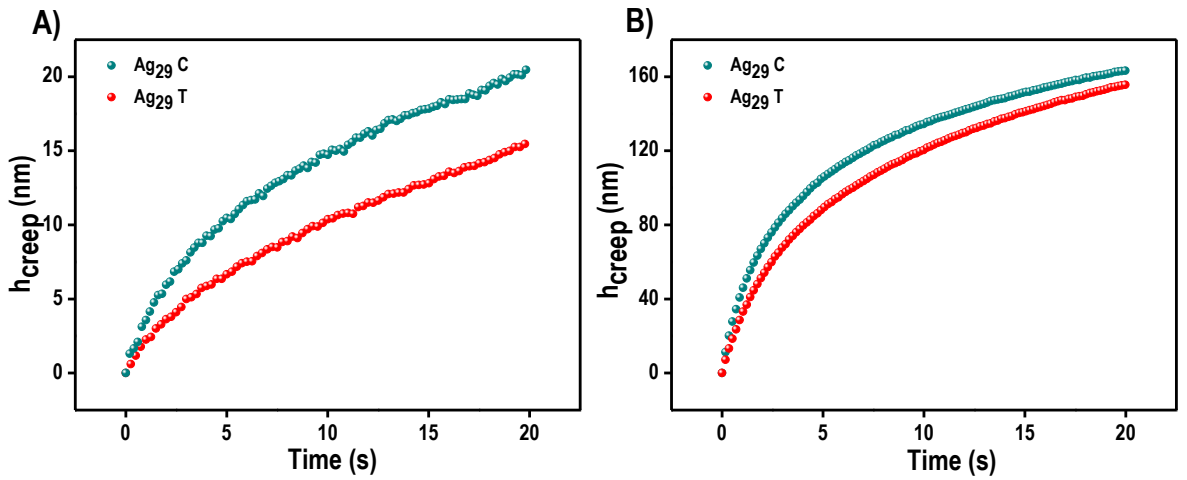

Figure S8. Experimental creep curves corresponding to Ag_{29} C (cyan trace) and Ag_{29} T (red trace) crystal system at a load of A) 500 µN and B) 10,000 µN, respectively.

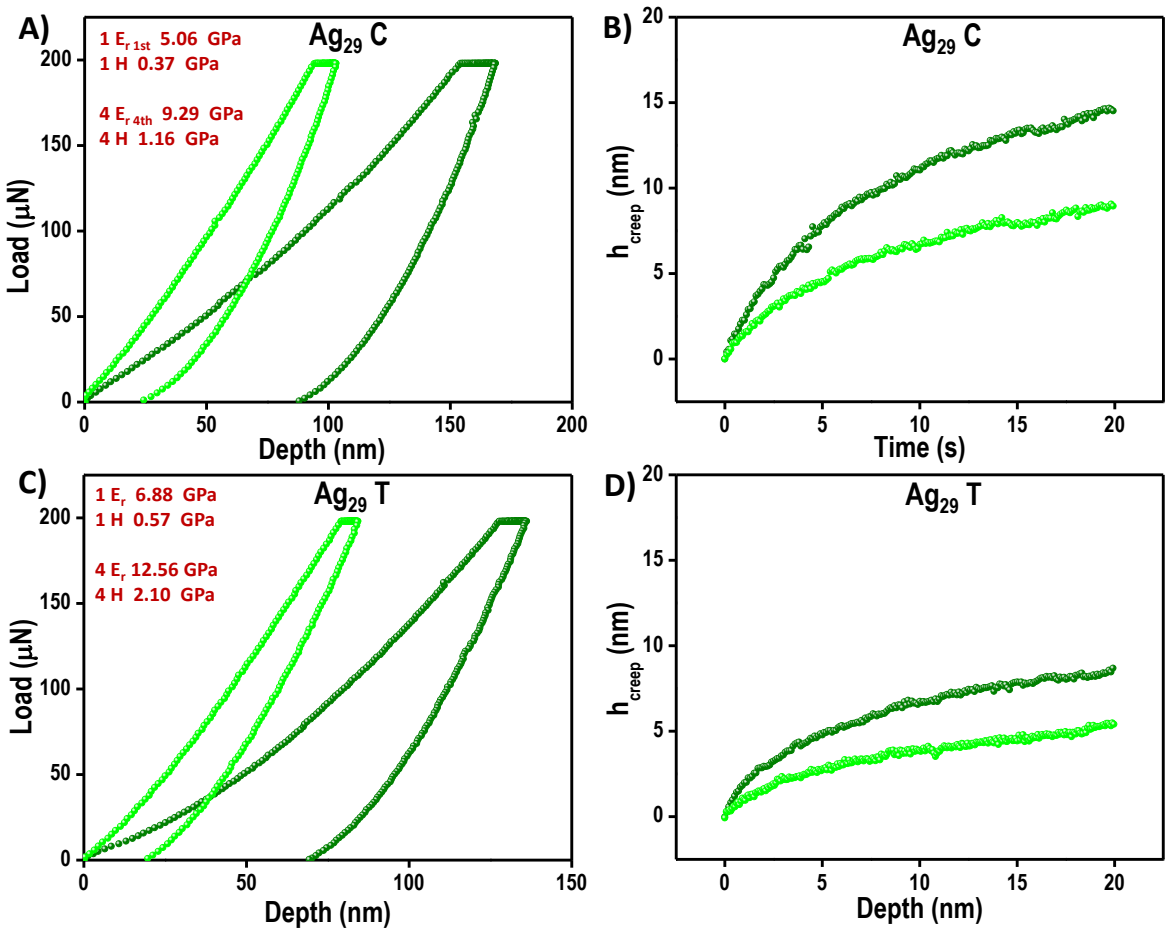

Figure S9. All single-crystal samples underwent the same experiment four times on the same indentation area. A) and C) are the load-displacement plots of Ag_{29} C and Ag_{29} T crystals (first cycle olive and fourth cycle green). B) and D) are the creep displacement plots of Ag_{29} C and Ag_{29} T (first cycle olive and fourth green). Corresponding E_r and H values are indicated. A significant reduction in creep displacement is observed for the fourth measurement indicating an increased resistance to plastic deformation. This observation is consistent with strain hardening.

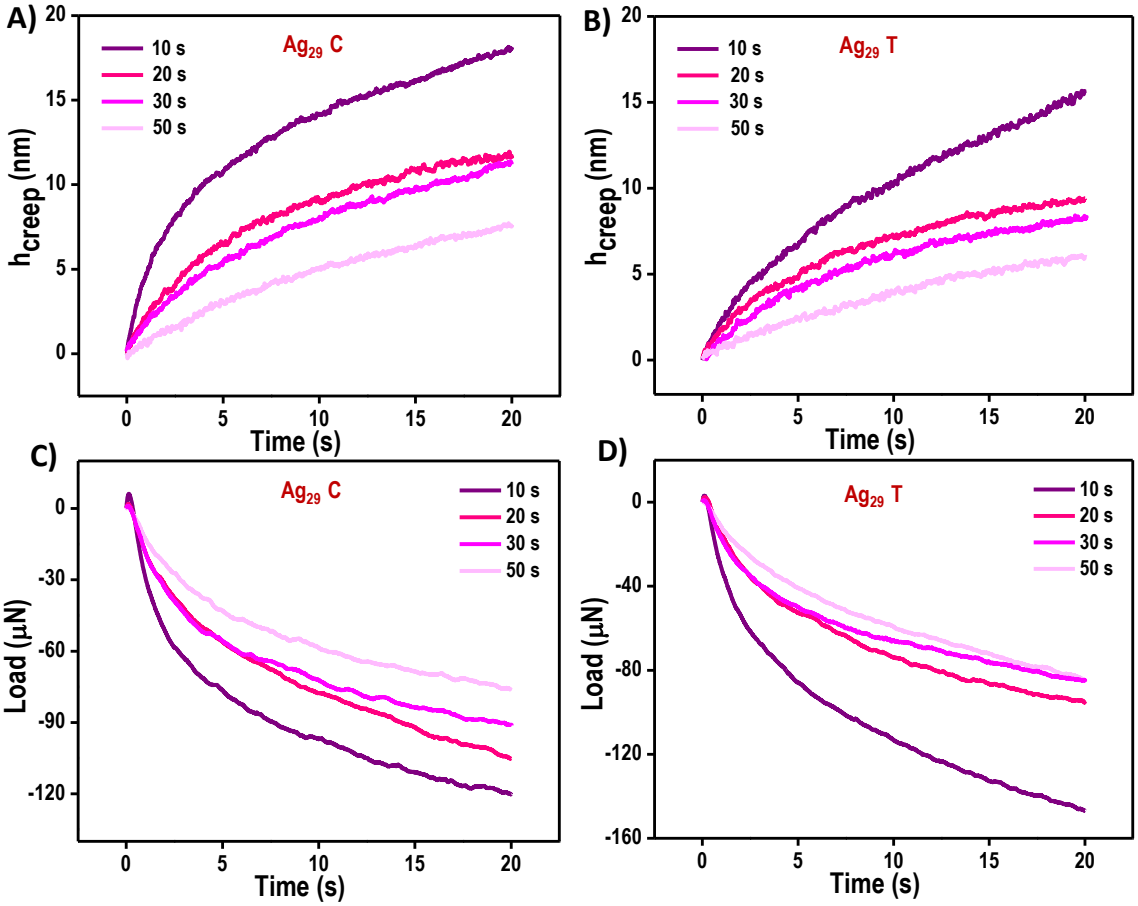

Figure S10. Experimental creep curves with loading rates of 20, 10, 6.6, and 4 µN/s (top A and B) and stress relaxation curves with displacement rates of 25, 12.5, 8.33, and 5 nm/s. (bottom C and D) corresponding to Ag_{29} C and Ag_{29} T crystal systems.

Modelling of stress-relaxation

The relaxation of the maximum load during holding to a certain depth is related to the time dependent, i.e., viscoelastic behaviour of the material. The instantaneous, i.e., elastic behaviour can be captured by a spring and the viscous behaviour can be depicted by a dashpot. A spring connected with a dashpot is called as a Maxwell element. One or more Maxwell element in parallel are used to model the stress relaxation of a material.

For a spherical indenter tip, the load–displacement relationship for a Hertzian elastic solid[1] is showed in equation [1]

$$P = 8G\frac{\sqrt{Rh^3(t)}}{3(1-\nu)} \qquad [1]$$

where G is the shear modulus, R is the indenter radius, ν is the Poisson's ratio, and h(t) is the displacement as a function of time. For the generalized Maxwell–Wiechert viscoelastic model,[2, 3] this equation can be rewritten in terms of a time-dependent relaxation modulus function, $G_{rel}(t)$, for the stress-relaxation response to an instantaneous ramp displacement, h_0.

$$P = 4G_{rel}(t)\frac{\sqrt{Rh_0{}^3}}{3} \qquad [2]$$

The stress relaxation data of the four CAS systems are fitted with two parameter Maxwell-Weichart model i.e., Figure S11. The total stress in the network will be the summation of the stress in individual arm. So, total stress σ

$$\sigma = \sigma_e + \sum_j \sigma_j \qquad [3]$$

So, the relaxation modulus $G_{rel}(t)$ is given by

$$G_{rel}(t) = \frac{\sigma}{\epsilon_0} = G_e + \sum_j G_j \exp(\frac{-t}{\tau_j}) \qquad [4]$$

The experimental data of four crystals have been plotted and fitted in two parameter Maxwell-Weichart model which is described in Figure S11. G_α is the relaxation modulus at t tends to infinity which is equal to G_e. G_0 is the value of instantaneous relaxation modulus, i.e., relaxation modulus at t=0 and which is $G_\alpha + \sum_j G_j$. The τ_1 and τ_2 are the primary and secondary relaxation times, i.e., the relaxation times of the first and second arm respectively.

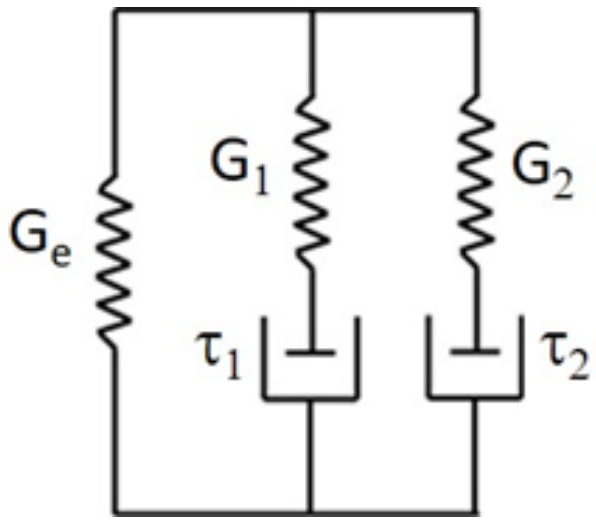

Figure. S11. Maxwell-Weichart model.

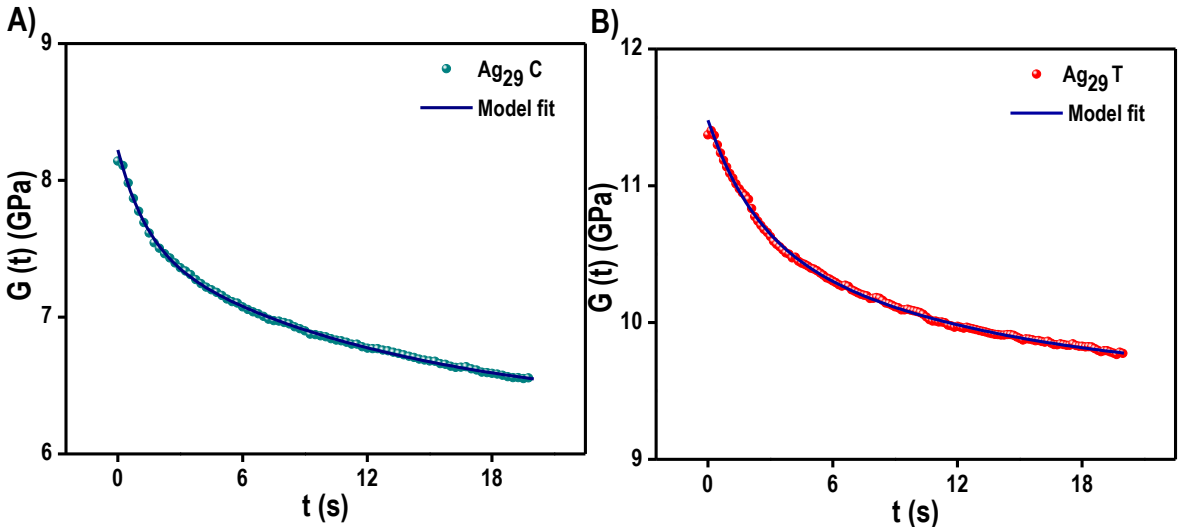

Figure S12. Experimental stress relaxation curves of A) Ag_{29} C and B) Ag_{29} T crystals fitted with the model (blue solid line) which captures the stress relaxation behaviour.

Table S2. G_0, G_α, τ_1 and τ_2 values of Ag_{29} C and T systems.

CAS	G_0 (GPa)	G_α (GPa)	τ_1 (s)	τ_2 (s)	R^2
Ag_{29} C	8.21	6.28	1.37	12.81	0.99
Ag_{29} T	11.50	9.58	12.16	2.22	0.99

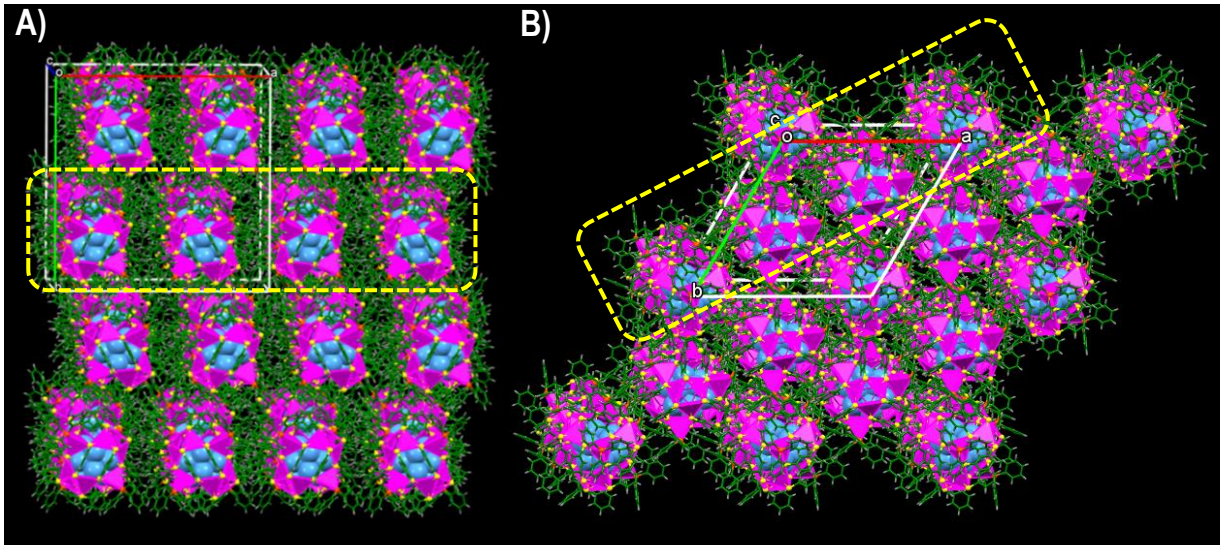

Figure S13. The 2x2x2 packing of A) Ag_{29} C and B) Ag_{29} T crystals showing linear arrangements of clusters (dotted yellow line). Color codes: cerulean/magenta, Ag; yellow, S; orange, P; green, C; grey, H.

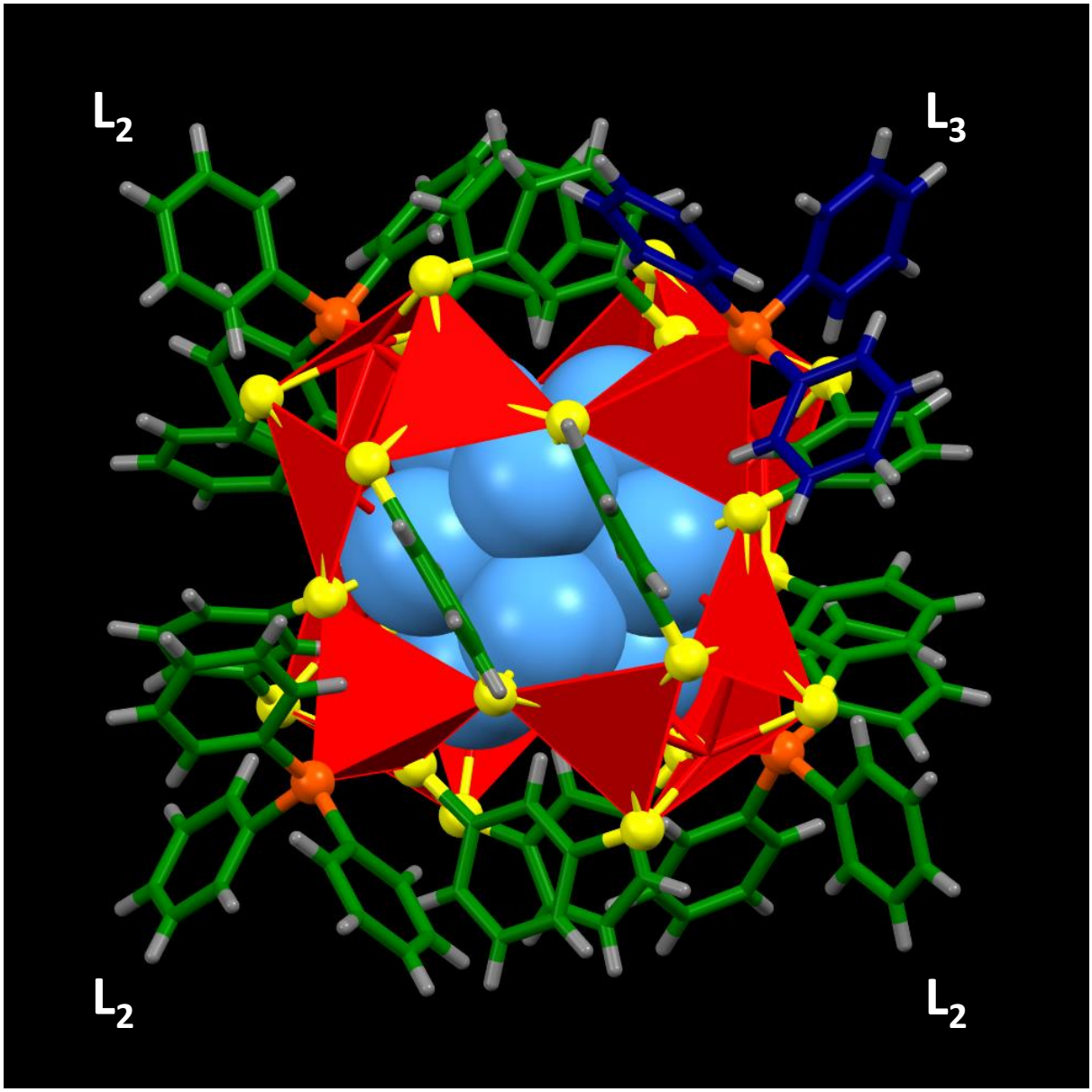

Figure S14. Total structure of Ag_{29} C with TPP ligand bundles in two ways: double-bundles (L_2) and triple bundles (L_3- blue trace) of CH...π interactions. Color codes: cerulean/red, Ag; yellow, S; orange, P; green/blue, C; grey, H.

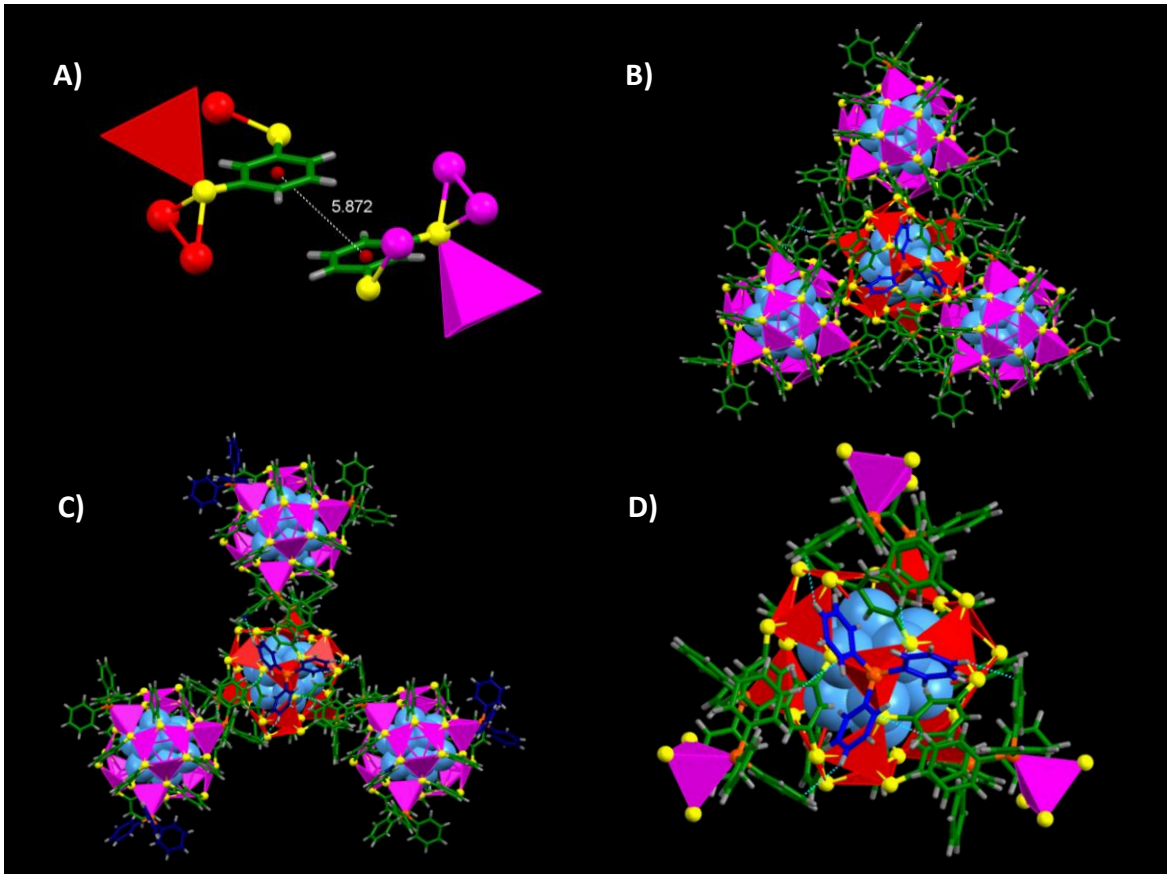

Figure S15. The intercluster interactions in Ag_{29} clusters in cubic lattice. A) The parallelly displaced π...π interactions between the BDT ligands of Ag_{29} clusters in cubic lattice. B) Intercluster CH...π interactions between the remaining three TPP ligands with other three clusters. C) and D) Intercluster CH...π interactions of one TPP ligand (highlighted in blue) with TPP ligands of three neighbouring clusters in cubic lattice. Color codes: cerulean/magenta/red, Ag; yellow, S; orange, P; green/blue, C; grey, H.

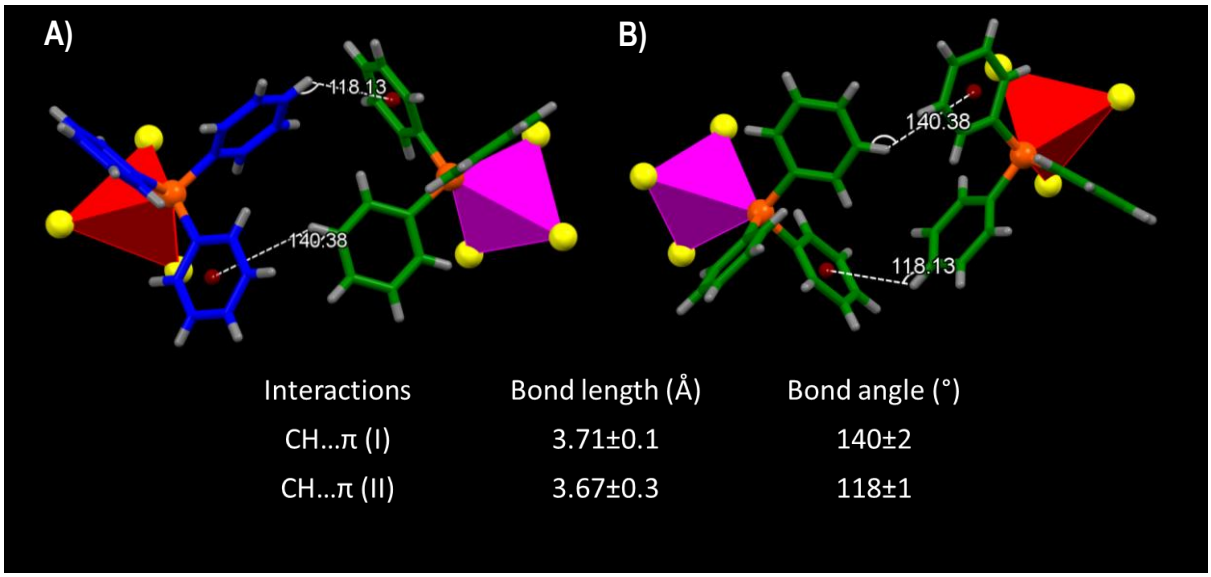

Figure S16. A) and B) shows the bond angle of the CH...π interactions in Ag_{29} cubic lattice. Color codes: magenta/red, Ag; yellow, S; orange, P; green/blue, C; grey, H.

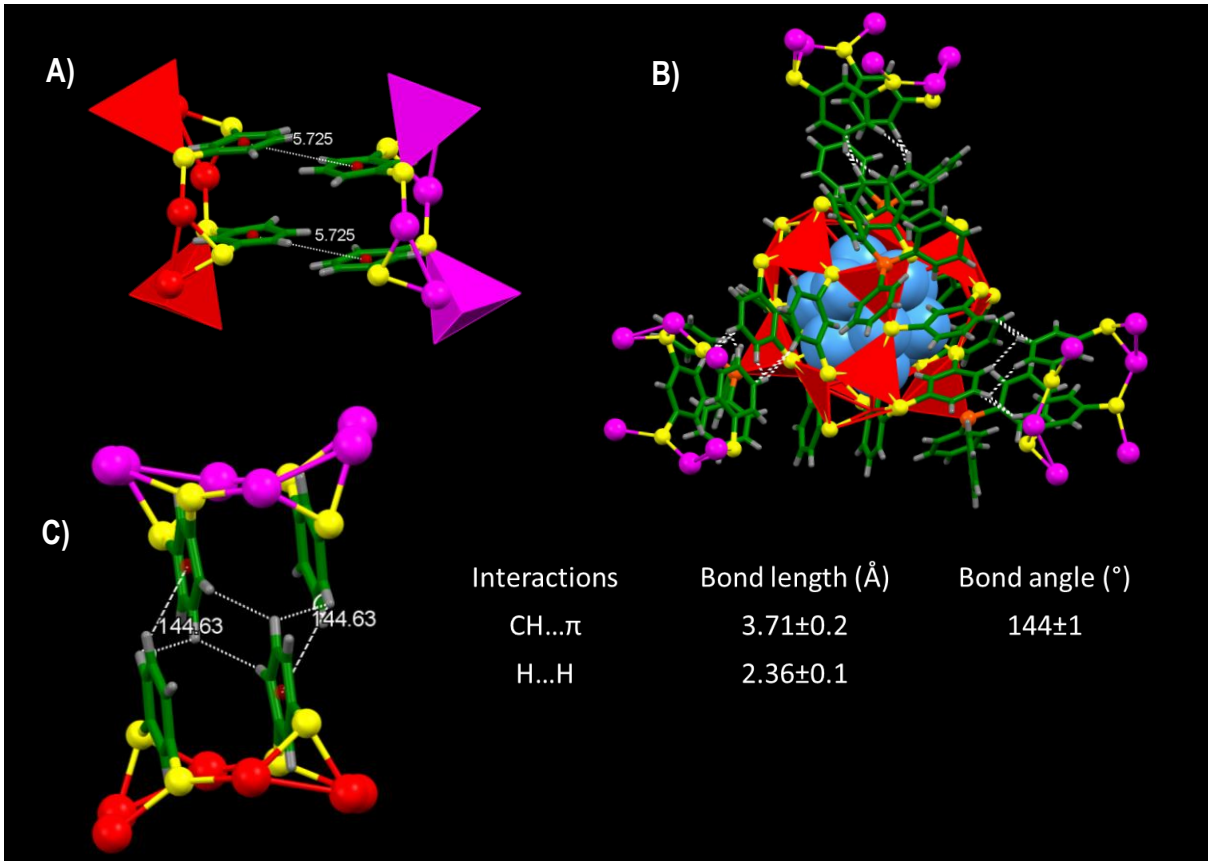

Figure S17. Supramolecular interactions of Ag_{29} clusters in trigonal lattice. A) The parallelly displaced π...π interactions between the BDT ligands of Ag_{29} clusters in trigonal lattice. B) The CH...π and H...H interactions in Ag_{29} T crystals. C) The bond angle of CH...π interactions between BDT ligands. Color codes: cerulean/magenta/red, Ag; yellow, S; orange, P; green, C; grey, H.

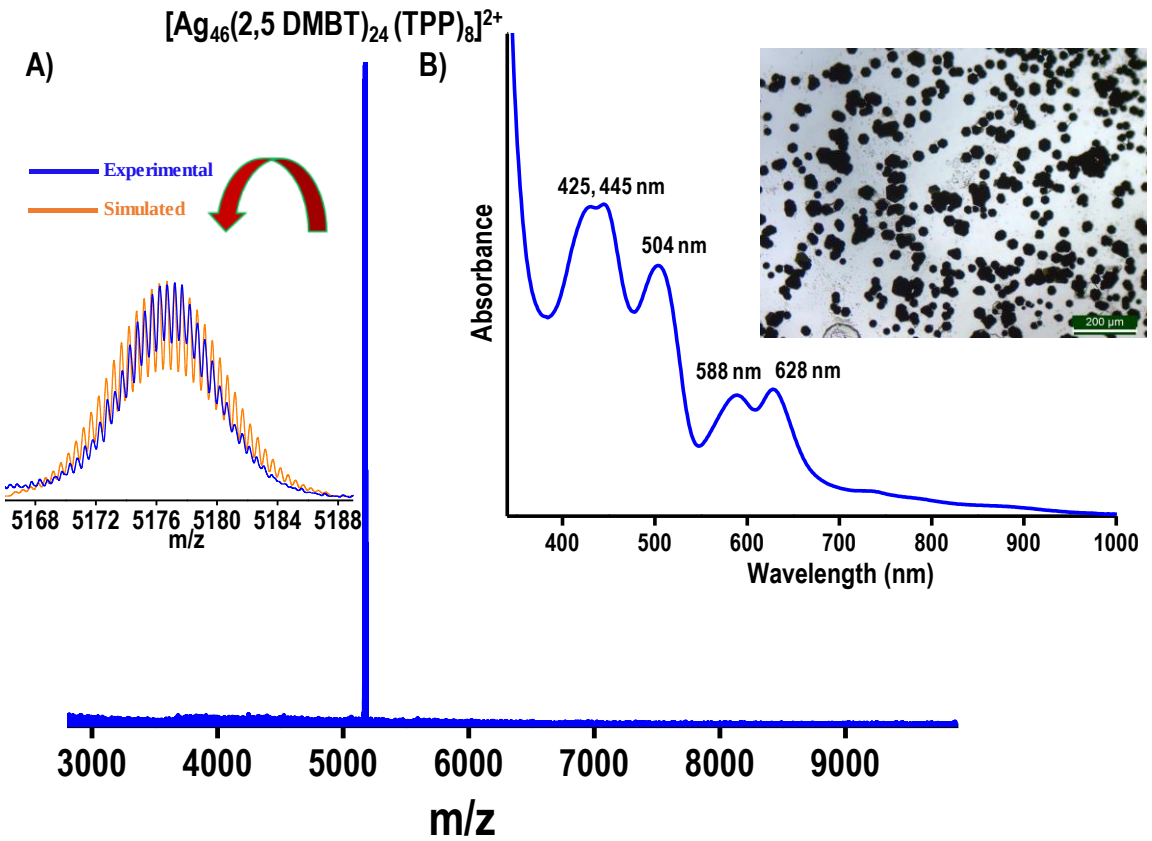

Figure S18. A) Full range ESI MS of clusters in positive ion mode. The peak is due to $[Ag_{46}(2,5\ DMBT)_{24}(PPh_3)_8]^{2+}$. Inset of A show the comparison of experimental (blue trace) and simulated (orange trace) isotopic distributions of the cluster. B) UV-vis absorption spectrum of the cluster in dichloromethane. Inset is the optical image of Ag_{46} T crystals in transmission mode.

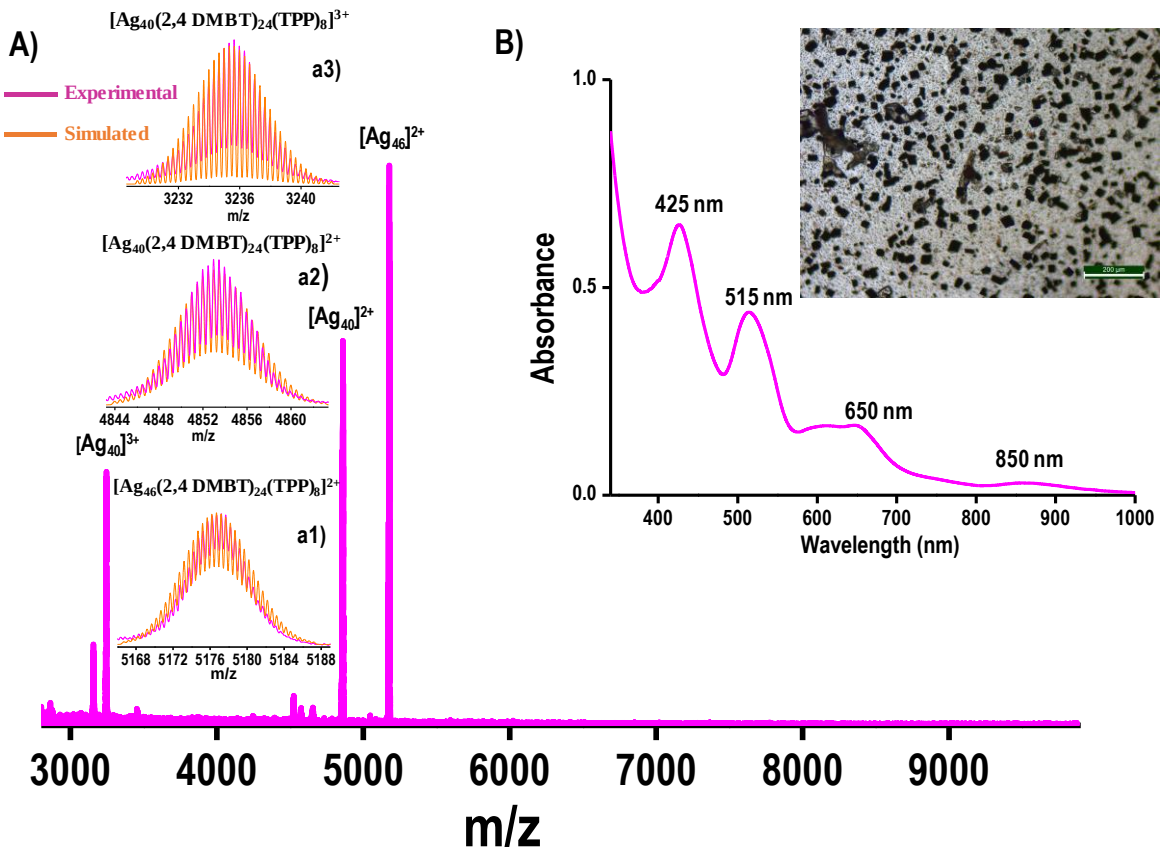

Figure S19. A) Full-range ESI MS of clusters in positive ion mode. The major peaks are due to Ag_{40}^{3+}, Ag_{40}^{2+}, and Ag_{46}^{2+}. The a1, a2 and a3 are the comparison of experimental (pink trace) and simulated (orange trace) isotopic distributions of Ag_{46}^{2+}, Ag_{40}^{2+}, and Ag_{40}^{3+}. B) UV-Vis absorption spectrum of the clusters in dichloromethane. Inset is the optical image of $Ag_{40/46}$ M crystals in transmission mode.

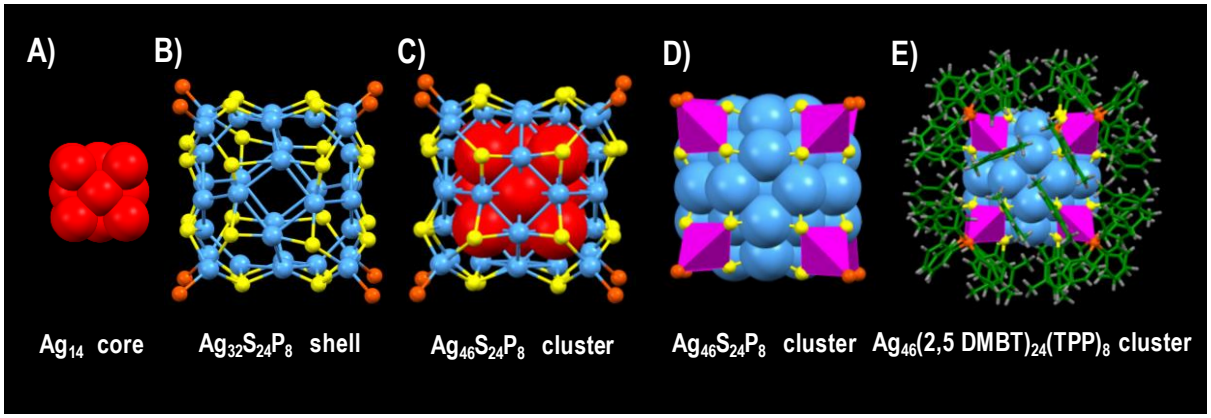

Figure S20. Structural anatomy of Ag_{46} T clusters. A) The Ag_{14} core; B) The $Ag_{32}S_{24}P_8$ motifs; C) and D) $Ag_{46}S_{24}P_8$ cluster in ball and stick and polyhedral model where the carbon tail of the ligands is omitted for clarity. E) The total structure of Ag_{46}(2,5 DMBT)$_{24}$(TPP)$_8$ clusters. Color codes: cerulean/magenta/red, Ag; yellow, S; orange, P; green, C; grey, H.

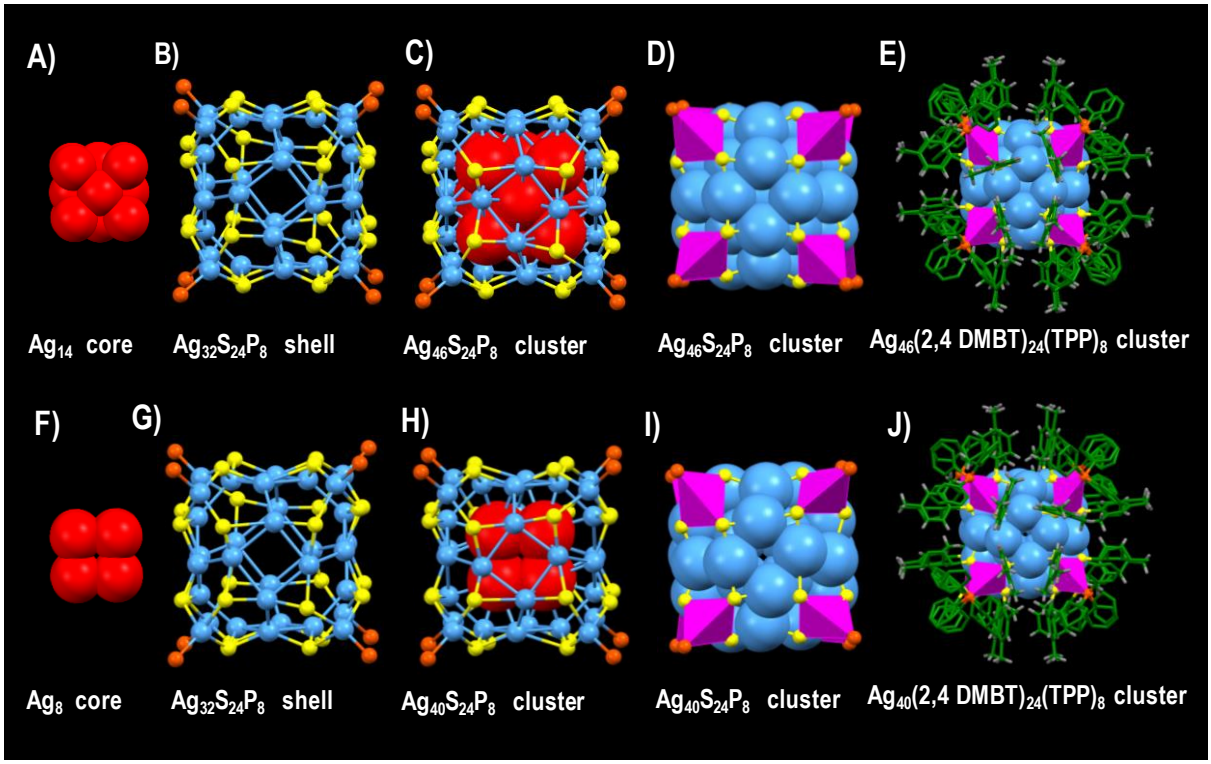

Figure S21. Structural anatomy of Ag_{46} and Ag_{40} clusters. A) and F) are the Ag_{14} and Ag_{8} inner core of Ag_{46} and Ag_{40} clusters; B) and G) are the $Ag_{32}S_{24}P_{8}$ shell that protects the inner cores of both Ag_{46} and Ag_{40} clusters; C) and H) are the $Ag_{46}S_{24}P_{8}$ and $Ag_{40}S_{24}P_{8}$ clusters in ball and stick model where the carbon tail of the ligands are omitted for clarity. D) and I) are the $Ag_{46}S_{24}P_{8}$ and $Ag_{40}S_{24}P_{8}$ clusters in polyhedral model. E) and J) are the total structure of Ag_{46}(2,4 DMBT)$_{24}$(TPP)$_{8}$ and Ag_{40}(2,4 DMBT)$_{24}$(TPP)$_{8}$ clusters. Color codes: cerulean/magenta/red, Ag; yellow, S; orange, P; green, C; grey, H.

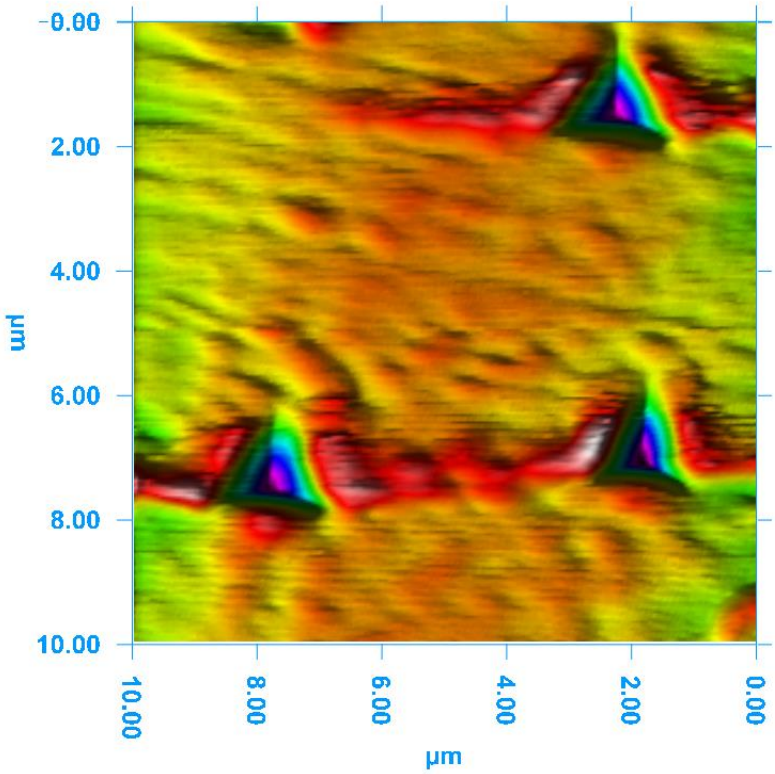

Figure S22. Piezo image showing residual indentation imprint on Ag_{46} T system.

Table S3 Measured E_r and H of Ag_{46} T and $Ag_{40/46}$ M compared with their ρ.

CASs	ρ (g/cm^{-3})	E_r (GPa)	H (MPa)
Ag_{46} T	1.322	2.27±0.25	168.10±25.52
$Ag_{40/46}$ M	1.497	2.73±0.51	166.70±28.02

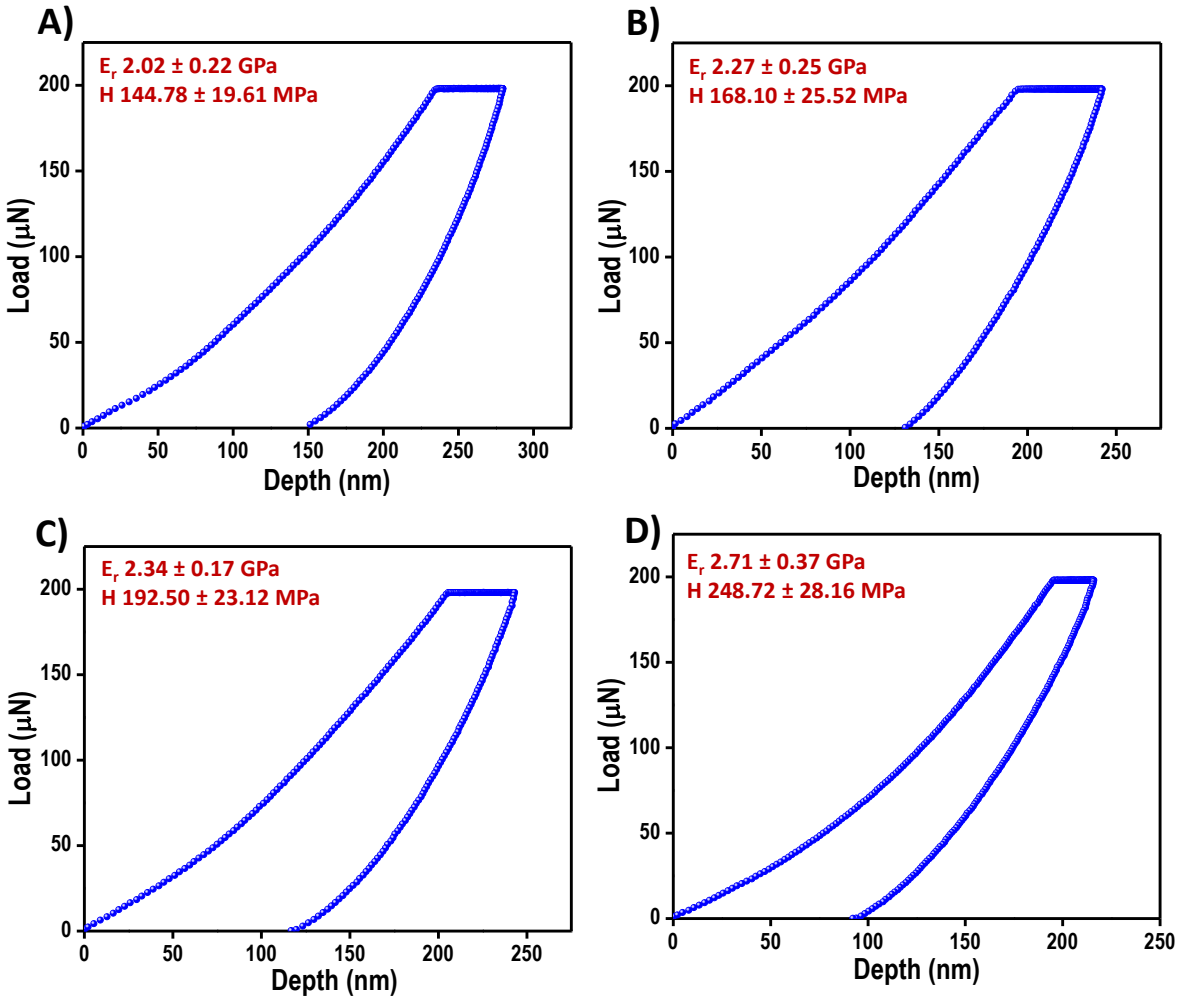

Figure S23. Load-displacement curves of $Ag_{46}T$ crystals with loading rates of A) 20, B) 10, C) 6.6, and D) 4 μN/s, respectively. The creep time of 50 s was used in this case to dissipate creep.

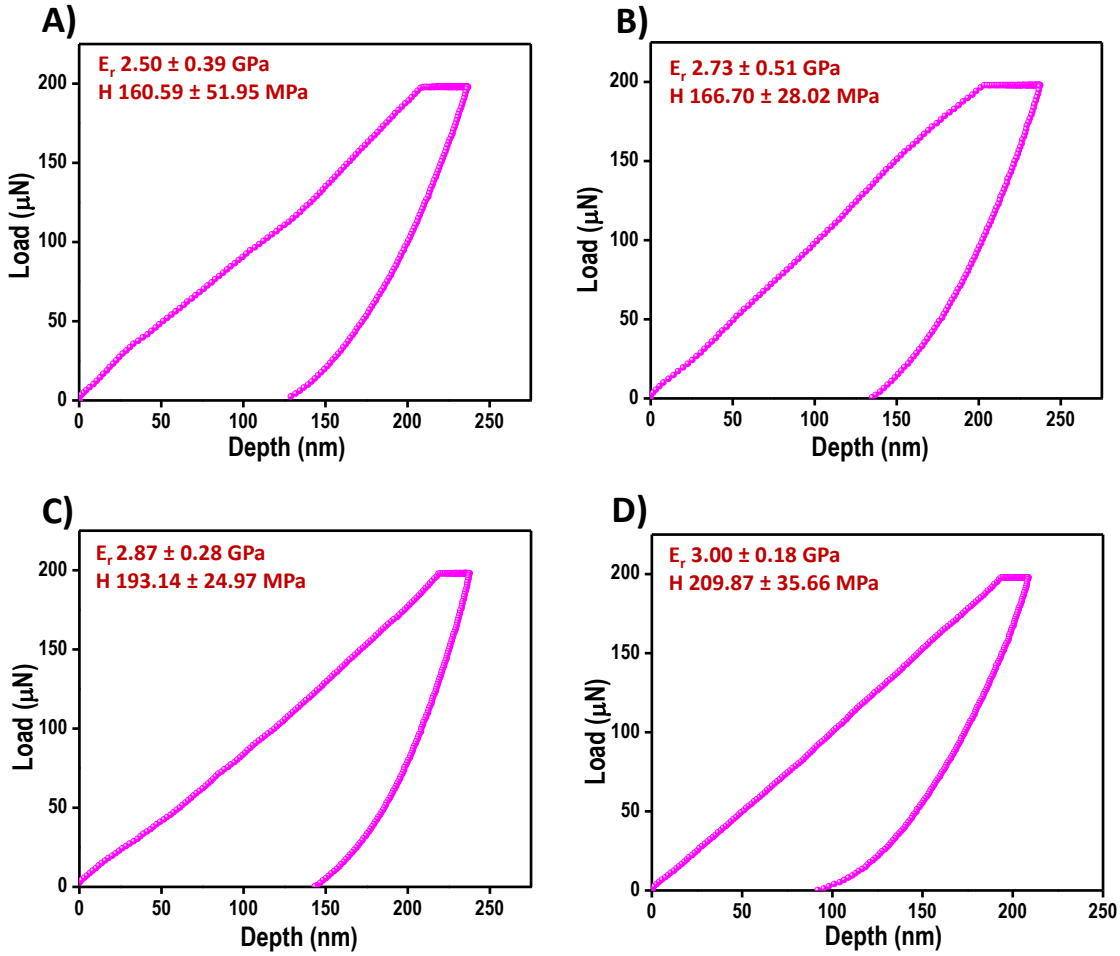

Figure S24. Load-displacement curves of $Ag_{40/46}$ M crystals with loading rates of A) 20, B) 10, C) 6.6, and D) 4 μN/s, respectively.

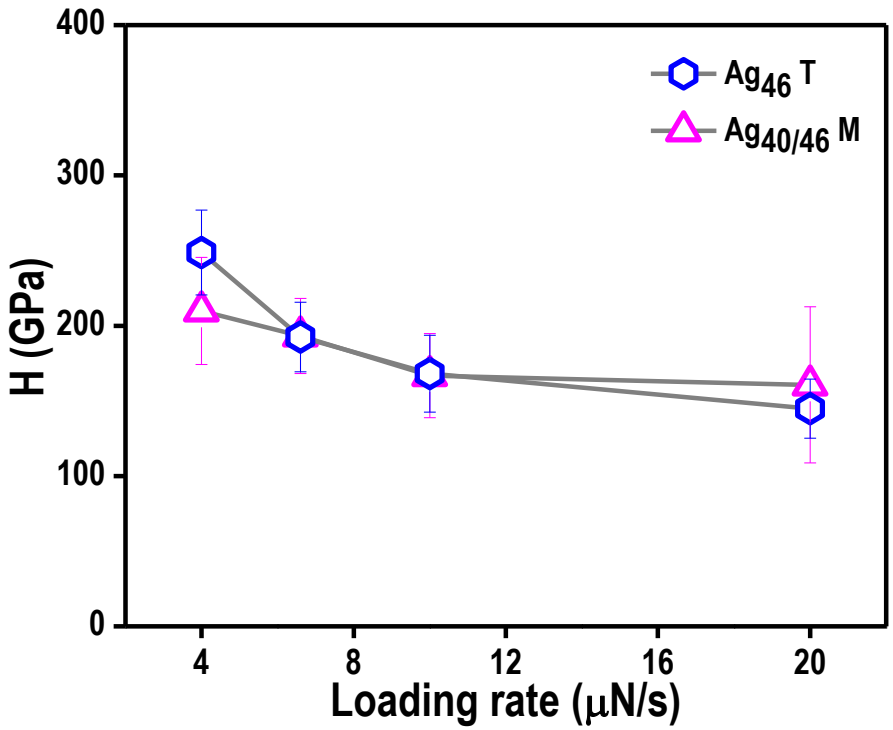

Figure S25. Variation of H with the loading rate of Ag_{46} T (blue trace) and $Ag_{40/46}$ M (pink trace) crystal systems

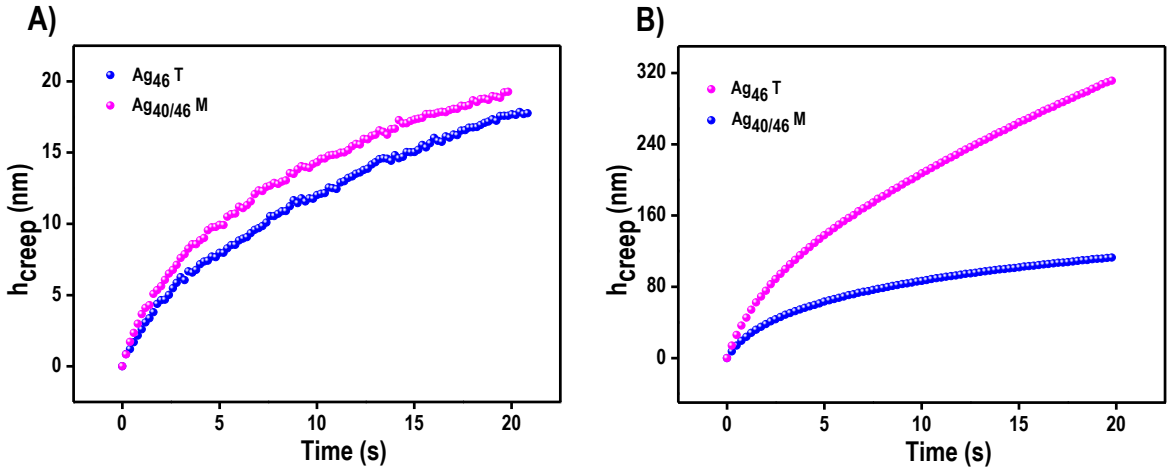

Figure S26. Experimental creep curves corresponding to Ag_{46} T (blue trace) and $Ag_{40/46}$ M (pink trace) crystal systems at a load of A) 500 µN and B) 10,000 µN, respectively.

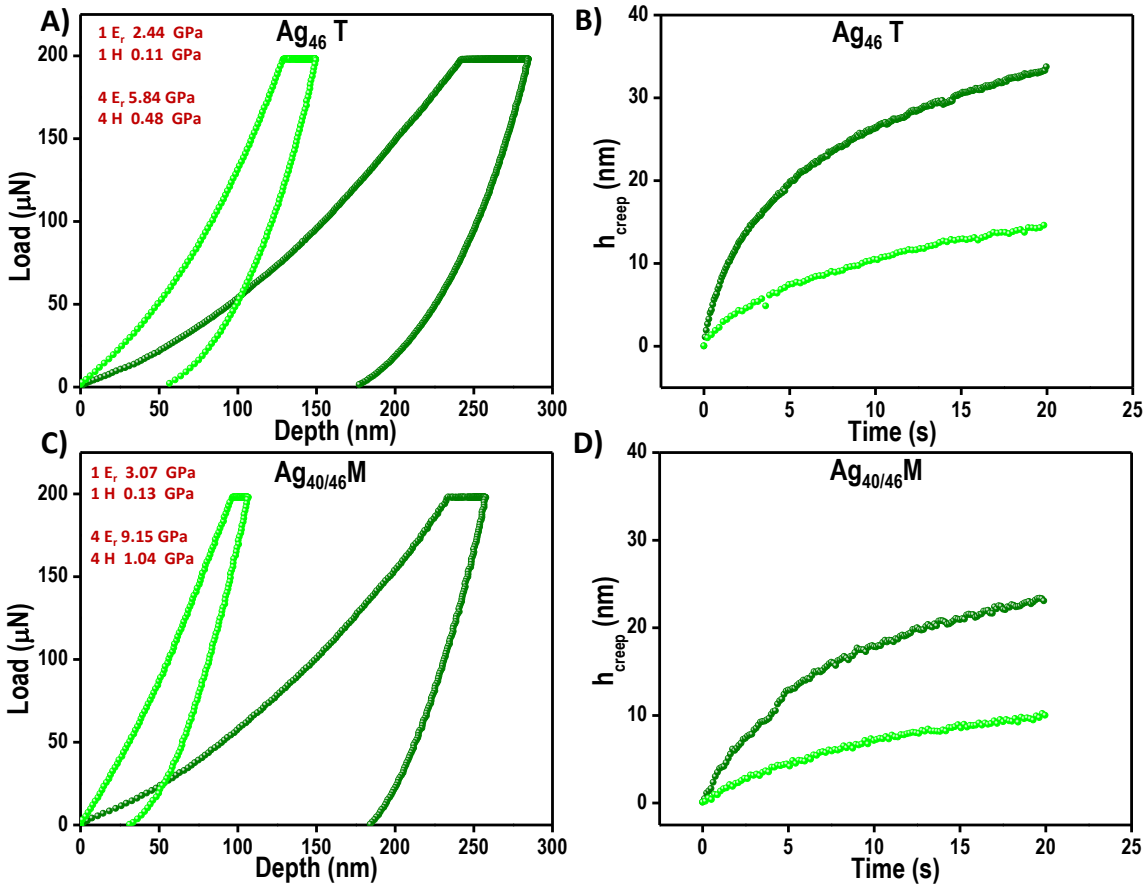

Figure S27. All single-crystal samples underwent the same experiment four times on the same indentation area. A) and C) are the load-displacement plots of Ag_{46} T and $Ag_{40/46}$ M crystals (first cycle olive and fourth cycle green). B) and D) are the creep displacement plots

of $Ag_{40/46}$ M and Ag_{46} T (first cycle olive and fourth green). Corresponding E_r and H values are indicated.

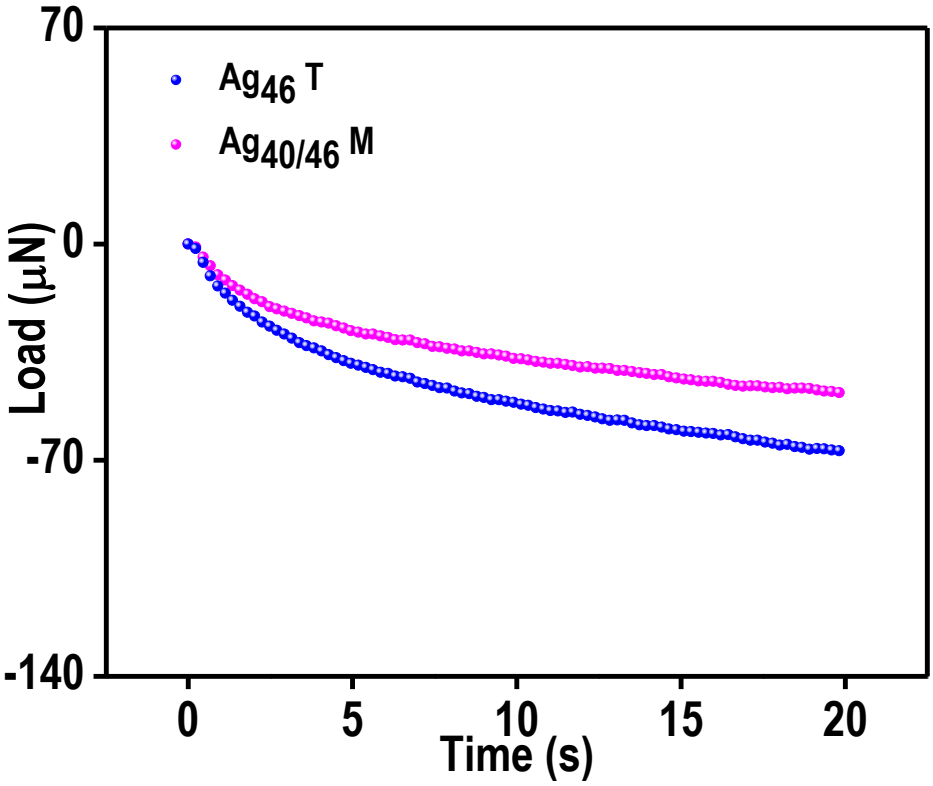

Figure S28. Stress relaxation plot of Ag_{46} T (blue trace) and $Ag_{40/46}$ M (pink trace) cluster crystals.

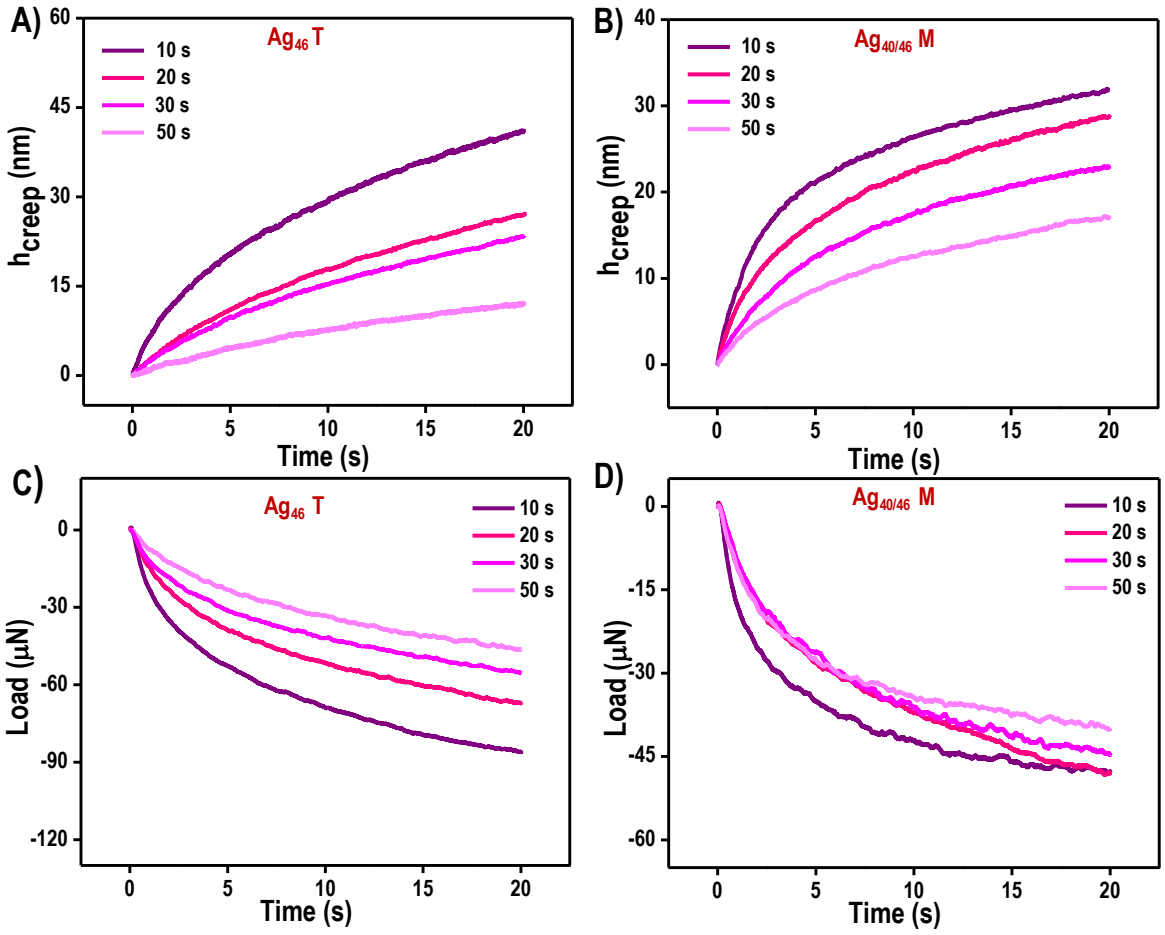

Figure S29. Experimental creep curves with loading rates of 20, 10, 6.6, and 4 µN/s (top A and B) and stress relaxation curves with displacement rates of 25, 12.5, 8.33, and 5 nm/s (bottom C and D) corresponding to Ag_{46} T and $Ag_{40/46}$ M crystal systems.

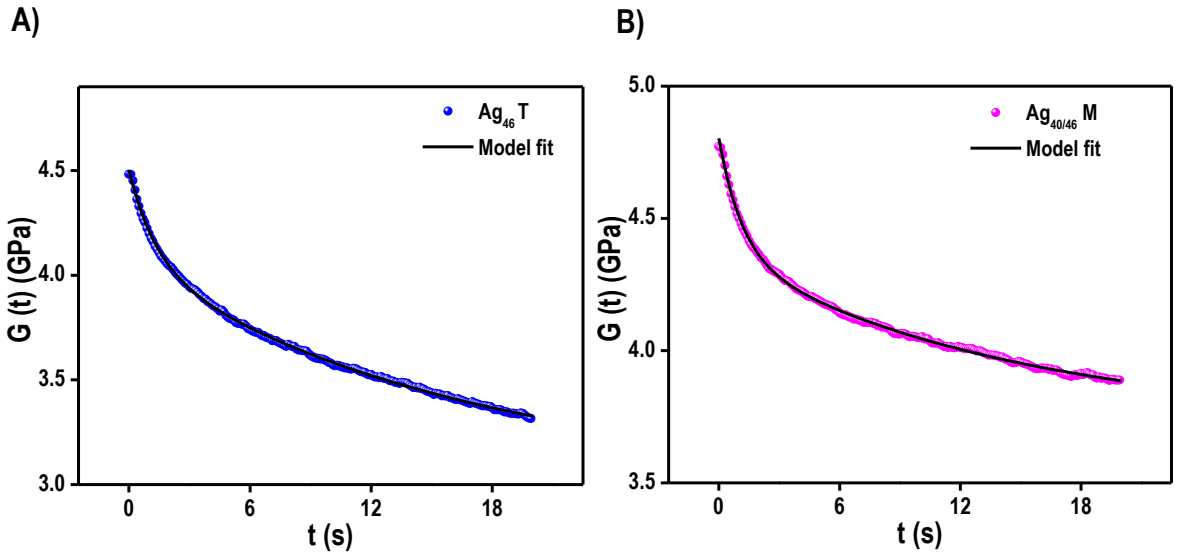

Figure S30. Experimental stress relaxation curves of A) Ag_{46} T and B) $Ag_{40/46}$ M crystals fitted with the model (black solid line) which captures the stress relaxation behaviour.

Table S4. G_0, G_α, τ_1, and τ_2 values of Ag_{46} T and $Ag_{40/46}$ M systems.

CASs	G_0 (GPa)	G_α (GPa)	τ_1 (s)	τ_2 (s)	R^2
Ag_{46} T	4.49	3.02	1.33	16.25	0.99
$Ag_{40/46}$ M	4.79	3.72	14.48	1.14	0.99

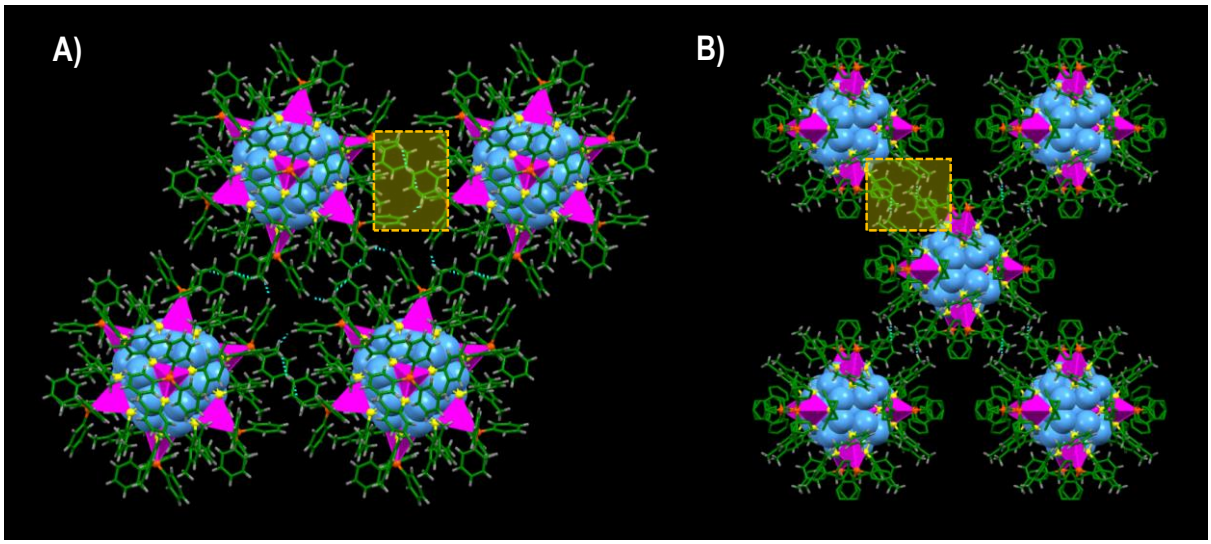

Figure S31. A) and B) Intercluster interactions of Ag_{46} T and $Ag_{40/46}$ M. Color codes: cerulean/magenta, Ag; yellow, S; orange, P; green, C; grey, H.

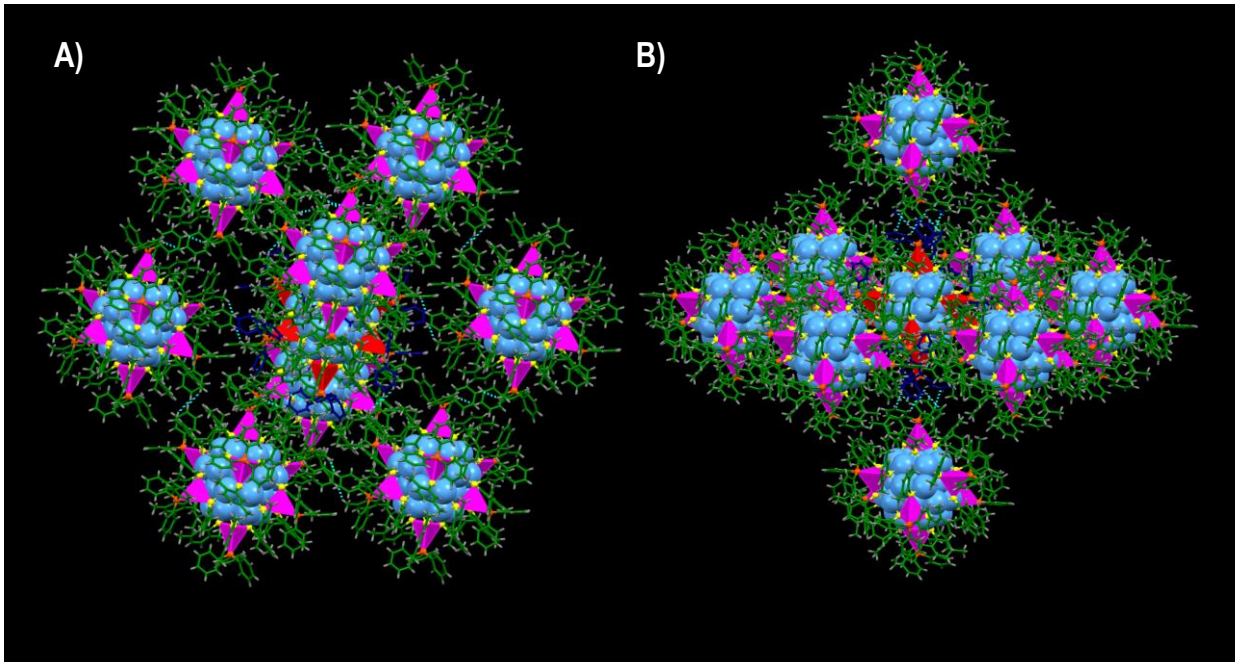

Figure S32. The supramolecular interactions in Ag_{46} T crystal. A) and B) shows different view of the interactions of each Ag_{46} cluster with eight neighbouring clusters in trigonal lattice. Color codes: cerulean/magenta/red, Ag; yellow, S; orange, P; green/blue, C; grey, H.

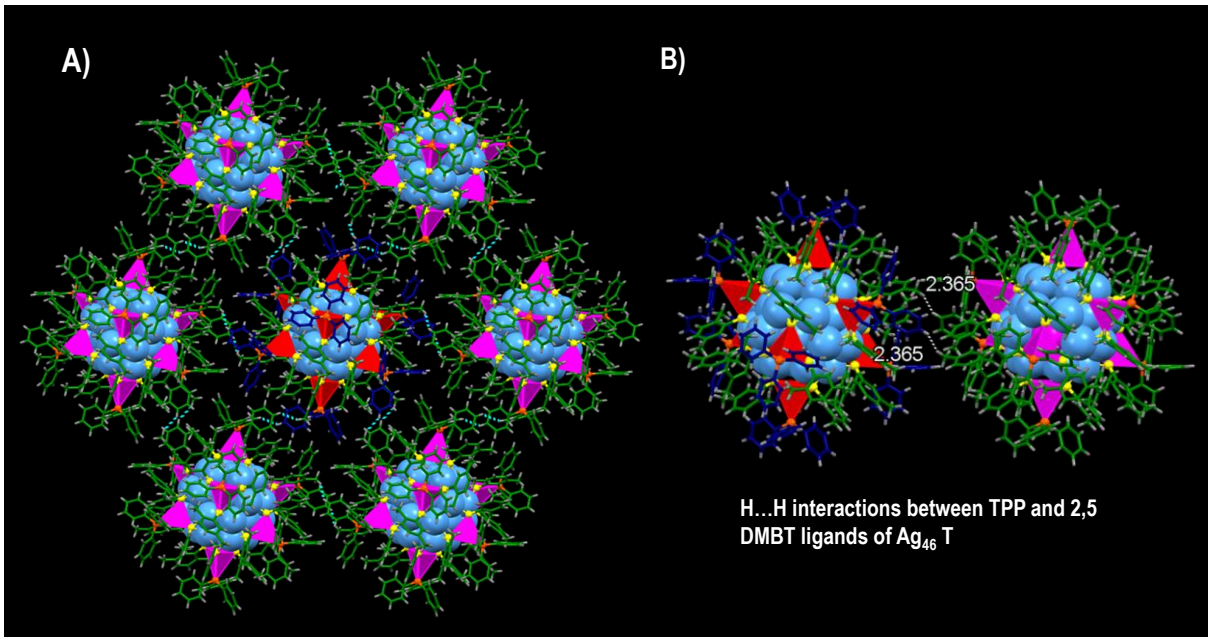

Figure S33. H...H interactions between TPP and 2,5 DMBT ligands in Ag_{46} T crystal. A) The view of H...H interactions between TPP and 2,5 DMBT ligands of Ag_{46} clusters with neighbouring six clusters. B) Shows the bond length of the H...H interactions. Color codes: cerulean/magenta/red, Ag; yellow, S; orange, P; green/blue, C; grey, H.

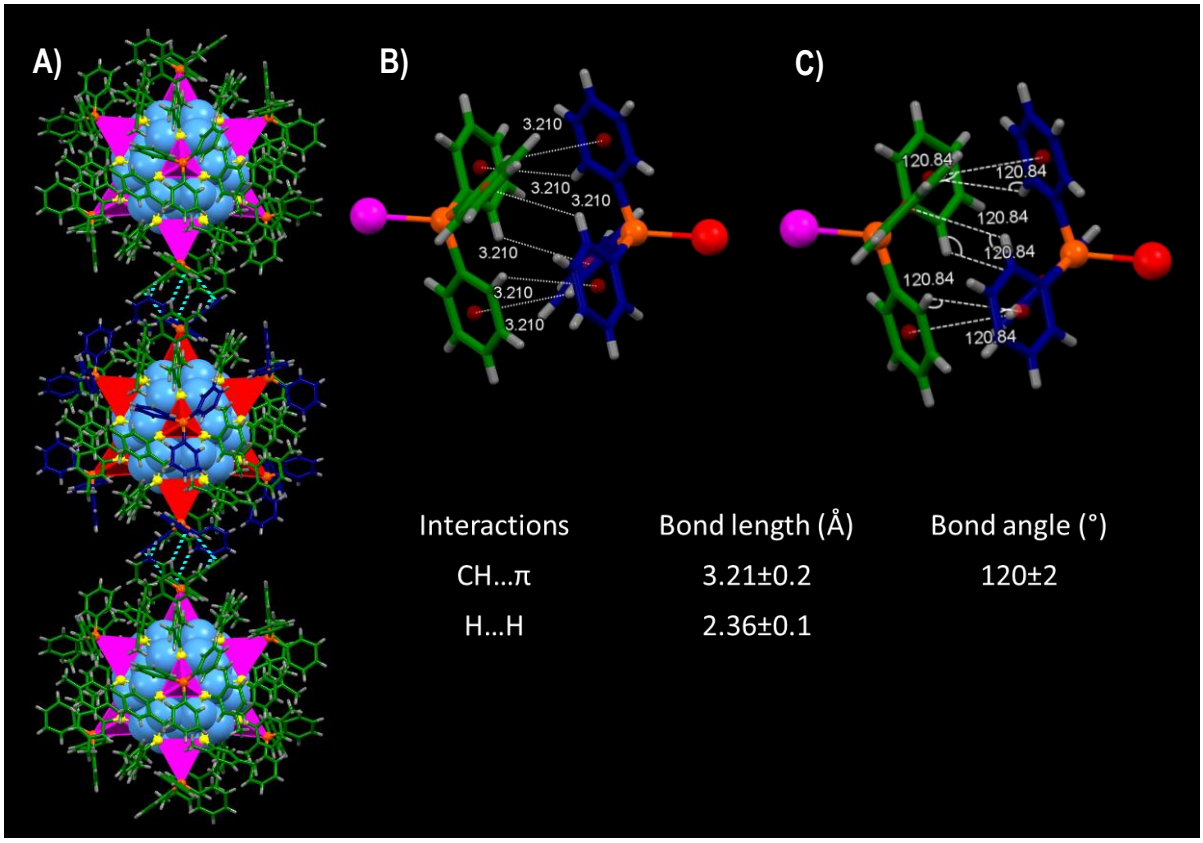

Figure S34. A) The six pair of CH...π interactions between the pole site TPP ligands in Ag_{46} T crystal. B) and C) shows the bond length and bond angle of six pair of CH...π interactions. Color codes: cerulean/magenta/red, Ag; yellow, S; orange, P; green/blue, C; grey, H.

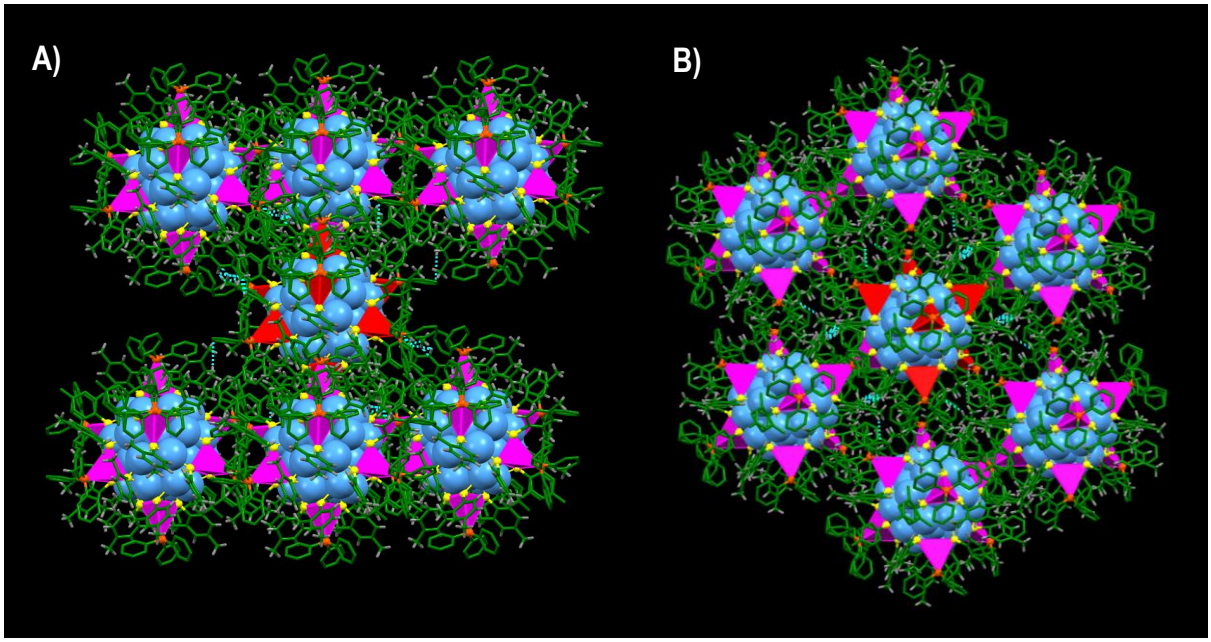

Figure S35. A) and B) shows the different view of the interaction of $Ag_{40/46}$ cluster with its neighbouring clusters in a monoclinic lattice. Color codes: cerulean/magenta/red, Ag; yellow, S; orange, P; green, C; grey, H.

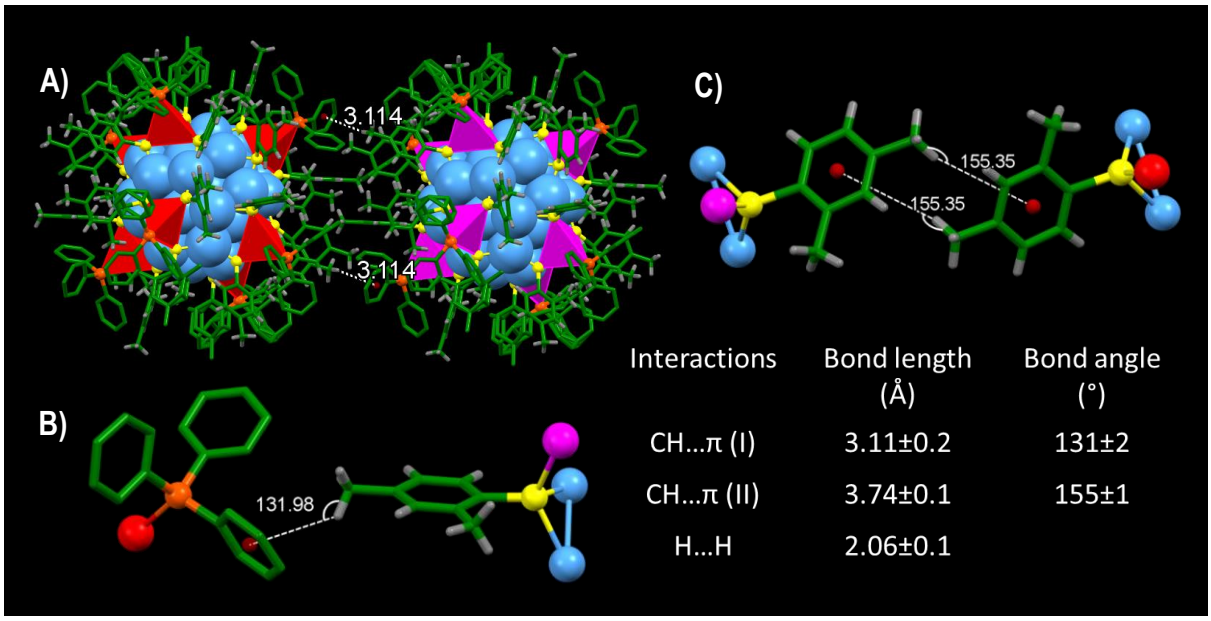

Figure S36. A) CH...π interactions between TPP and 2,4 DMBT ligands. B) The bond angle of CH...π interactions between the TPP and 2,4 DMBT ligands in the monoclinic lattice. C) The bond angle of the CH...π interactions between two 2,4 DMBT ligands in the monoclinic lattice. Color codes: cerulean/magenta/red, Ag; yellow, S; orange, P; green, C; grey, H.

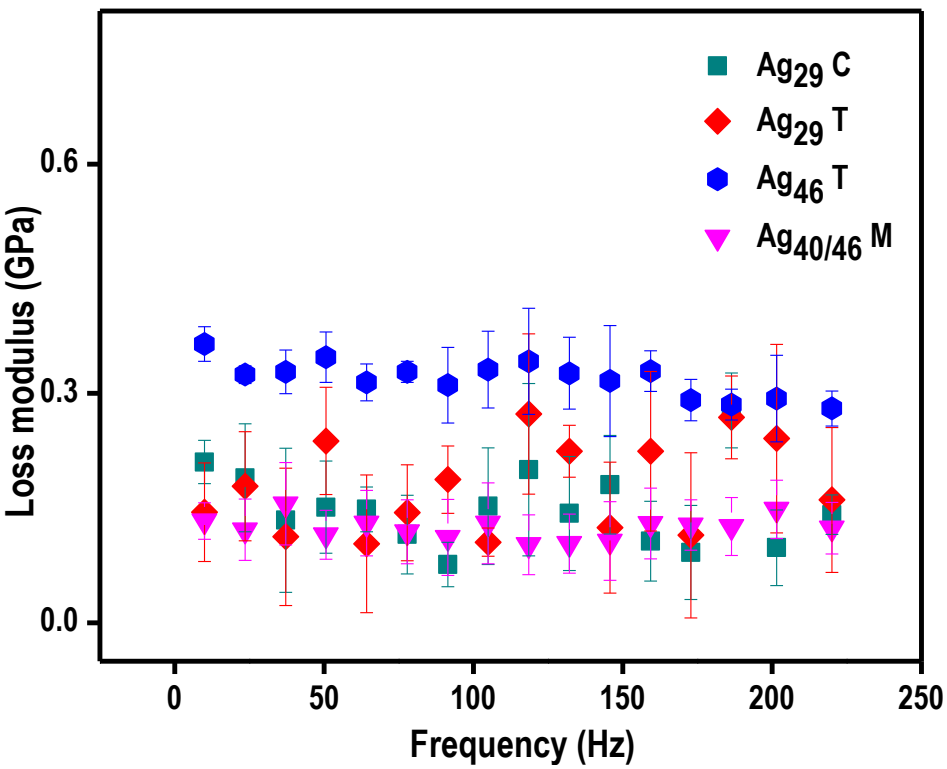

Figure S37. Variation of loss modulus with frequency of Ag_{29} C (cyan trace), Ag_{29} T (red trace), Ag_{46} T (blue trace), and $Ag_{40/46}$ M (pink trace).

References

1. Cheng, L.; Xia, X.; Scriven, L. E.; Gerberich, W. W., Spherical-tip indentation of viscoelastic material. *Mechanics of Materials* **2005,** 37, (1), 213-226.
2. Kaufman, J. D.; Miller, G. J.; Morgan, E. F.; Klapperich, C. M., Time-dependent mechanical characterization of poly(2-hydroxyethyl methacrylate) hydrogels using nanoindentation and unconfined compression. *Journal of Materials Research* **2011,** 23, (5), 1472-1481.
3. Roylance, D.; Cohen, K. C.; Jenkins, C. H.; Khanna, S. K., Mechanics of materials: A materials science perspective. *Proceedings of the Institution of Mechanical Engineers, Part L: Journal of Materials: Design and Applications* **2001,** 215, (3), 141-145.